جامعة أبو بكر بلقايد
UNIVERSITÉ DE TLEMCEN

Pan African University
Institute of Water and Energy Sciences

Institute of Water and Energy Sciences (Including Climate Change)

Application of Satellite Rainfall Products for the Assessment of Water Availability in Ethiopian Highlands: The Case of Ribb Watershed

Mulugeta Ferede Melese

Date: 06/ 09 / 2017

Master in Water, Engineering track

Research Supervisor

Seneshaw Tsegaye (PhD), Florida Gulf Coast University, USA

President

Prof. Dr. Mihert D. Ulsido

External Examiner

Prof. Chaibi Thameur

Internal Examiner

Dr. Bouchelkia Hamid

Academic Year: 2016-2017

Declaration

I Mulugeta Ferede, hereby declare that this thesis represents my personal work, realized to the best of my knowledge. I also declare that all information, material and results from other works presented here, have been fully cited and referenced in accordance with the academic rules and ethics. The authors email is mulef23@gmail.com or mulugetaferd@gmail.com.

Abstract

One of the versatile use of satellite rainfall products is provision of continuous information which can be used for the assessment of water availability in the data sparse areas. Primarily, we compared the performance of TRMM 3B42 version 7 & CMORPH rainfall with Ribb rain gauge stations on the monthly timescale at the watershed scale. The TRMM 3B42 and CMORPH rainfall have shown similar strong PCC for both (0.99) and R^2, 0.98 and 0.97, respectively compared to the rainfall Ribb stations. Both rainfall products are portrayed consistent underestimation evidenced by their bias results, 25.54% and 23.78%, respectively. The errors embedded in TRMM 3B42 V7 and CMORPH rainfall proved by their RMSE values 57.05 and 45.67, respectively. The RMSE% values of TRMM 3B42 V7 and CMORPH are found to be 47 and 37.75, respectively. The SUFI-2 algorithm in SWAT CUP was employed to quantify the parameter sensitivity and predictive uncertainty and we found 8 most sensitive parameters. Then, we obtained the acceptable p-factor and r-factor results, 0.85, 0.65, on calibration and 0.44, 0.28, on validation, respectively. Generally, the performance of SWAT model evaluation results on a monthly time step disclosed in the overall calibration and validation are very good in terms of NSE, R^2 and PBIAS with calibration values 0.91,0.92 and 6.1 and validation values 0.85,0.85 and 5.8, respectively. Lastly, we appraised on the water availability of the Ribb watershed through simulated water balance components using both rainfall products. The simulated surface runoff contribution to total flow was found to be very high as compared to the lateral flow. The significant amount of water was lost through evapotranspiration. The overall results of this study can be used for hydro-climatological operations & researches, and could provide an insight to the sustainable water resources development and water management in Ribb and similar watersheds.

Keywords: SWAT, Ribb watershed, Satellite rainfall products, hydrological Modeling, Sensitivity and Uncertainty Analysis.

Acknowledgments

First and foremost, thanks to the almighty of God for granting me with his limitless sympathy, love and blessings throughout my life.

I would like to express my deepest gratitude to my supervisor Dr. Seneshaw Tsegaye for his valuable comments, suggestions and continuous encouragements. Even if the research time was short, it was the best opportunity for me to work with you. Hopefully, our communication will continue in the future.

My special thanks go to Mr. Mohamed Zeko and Mr. Dejene Sahalu for their genuine supports and provision of all necessary research materials, data, and software's for this research work.

Most importantly, I would like to thank for all EIWR communities and especially Mr. Taffere Addis for his nice friendship.

None of this research would have been possible without the contribution of many people, However, impossible to list all of you here in the limited letters. Thus, thank you all for your great help on my personal cases and for this research too.

I would like to thank Pan African University for the scholarship and University of Tlemcen for hosting me.

I also thank all staff members of PAUWES, and Algerians for their hospitality.

I thank the National Meteorology Agency of Ethiopia and Ministry of Water, Irrigation and Electricity of Ethiopia for providing me all the necessary data used for this research work.

I would like to gratitude to Dr. Tena Alamirew and Water and Land Resource Centre (WLRC), Addis Ababa University (AAU) staffs for allowing me to conduct my internship program at your renowned institutions.

Finally, my sincerest thanks to my entire family for their true love, care, and prayers gave me strength to go on.

Table of Contents

Lists of Abbreviations and Symbols

BCM	Billion Cubic Meter
Bsn	Basin
CMORPH	Climate Prediction Center morphing technique
CN	Curve number
Dd	decimal degree
DEM	Digital Elevation Model
ET	Evapotranspiration
FAO	Food and Agriculture Organization
GIS	Geographical Information System
GSA	Global Sensitivity Analysis
Gw	Groundwater
HRU	Hydrologic Response Unit
HWSD	Harmonized World Soil Database
ITCZ	Intertropical Convergence Zone
LATF	Lateral Flow
Lat	Latitude
LH-OAT	Latin hypercube one-factor-at-a-time
Lon	Longitude
LULC	Land Use and Land Cover
Mgt	Management
Mm	Millimeter
MoWIE	Ministry of Water Irrigation and Electricity of Ethiopia
MW	Microwave
NA	Not Available
Netcdf	Network Common Data Format
NMAE	National Meteorology Agency of Ethiopia

NSE	Nash-Sutcliffe Model Efficiency
PBIAS	Percent of bias
PCC	Pearson correlation coefficient
PCP	Rainfall
PET	Potential Evapotranspiration
PPU	Percent Prediction Uncertainty
R^2	Coefficient of Determination
RH	Relative Humidity
S. N	Serial Number
SCS	Soil conservation services
Sol	Soil
SRE	Satellite Rainfall Estimate
SRPs	Satellite Rainfall Products
SUFI2	Sequential Uncertainty Fitting Two
Sun hr	Sunshine Hour
SURF	Surface Runoff
SWAT	Soil and Water Assessment Tool
SWAT CUP	SWAT Calibration and Uncertainty Program
TMax	Maximum Temperature
TMin	Minimum Temperature
TMPA	Multi-Satellite Precipitation Analysis
TRMM	Tropical Rainfall Measuring Mission
USSCS	United States Department of Agriculture Soil Conservation Service
UTM	Universal Transverse Mercator
WBC	Water Balance Components
Ws	Wind speed
WY	Water yield

Lists of Tables

Lists of Figures

This Thesis work is dedicated to

the

memory of my beloved Daddy

Ferede Melese

CHAPTER ONE

1. Introduction

Ethiopia is blessed with the abundance of water resources potential which is known as the water tower of the Horn of Africa. Many rivers in Ethiopia are originated from highland and high rainfall areas and then they generate a substantial amount of runoff to the river basin system (Melesse et al., 2014). Ethiopia's annual surface and ground fresh water availability potential was estimated approximately 123 and 2.6 BCM, respectively (Birhane, 2002). Unfortunately, the agriculture sector, which is the mainstay livelihood of the Ethiopian's economy, still not much benefited out of this plentiful water resource potential rather than relying on rainfall. Mostly in the highland area, the variability of rainfall is usually controlled through nonlinear interaction between a number of factors alike local orientation of altitude, slope and aspect (Haile et al., 2009). It is obvious that, the rainfall has its own contributions for the water availability in a certain area and similarly influenced by the interaction of the hydrologic systems. Quantifying water resources availability is still an ambiguous issue attributed to the lack of clear cut universal framework that can be pragmatic in quantifying the water availability in a certain region (Steduto et al., 2012). Accordingly, we appraised the water availability of Ribb watershed in terms of simulated streamflow and water balance components using the application of satellite rainfall products.

In order to have a reasonable representative estimation of water availability in terms of water balance (rainfall-runoff relationship) at watershed level the surface based measurement networks should be placed large enough that is the watershed area per numbers of gauges preferred to be small. Nevertheless, the availability and existence of the ground measuring stations are relatively limited in Ethiopia highlands. Owing to the undulating nature of the topography of Ethiopia highlands hampers them inaccessible, expensive to construct and tough to undertake regular maintenance. Hence, there might be inconsistent of among the records and also in some area totally

unavailable. Thus, satellite rainfall products can also be used to overcome these challenges.

Recently, in the advent and advancement of global satellite technology provides an optional high-resolution satellite rainfall products dataset. In the past two decades, the application of SRE algorithms became an appealing mechanism for the rainfall measurement (Moazami et al., 2013). High resolution satellite rainfall products can be used as an input for hydrological modeling works during lack of gauged data on the ground. As per (Hong et al., 2007; Jiang et al., 2012) findings the suitability of the satellite rainfall products (SRPs) for the particular region of interest has to be checked because of their indirect nature of the measurements of rainfall. In this thesis work, we used two widely used high-resolution satellite the measurements of which are of the TMPA adjusted product of version 7 (3B42V7) and CMORPH along with the Ribb watershed rain gauge data. The satellite rainfall products were compared with rain gauge data in the watershed.

Hydrological models are an indispensable tool for offering a common platform for experts, decision-makers and stakeholders (Weedon et al., 2011). However, their potential use in developing country is mainly constrained by data scarcity. In order to model and get a plausible water resource availability information from hydrological modeling works, the input of climate dataset like rainfall and evaporation must be accurate enough (Hughes, 2006). Understanding the fundamental connection within the hydrological components, mainly rainfall runoff process in the watershed could give pertinent clues for sustainable water resources utilization and management. Then, we evaluated the performance of semi-distributed hydrological model i.e. (Soil and Water Assessment Tool) through rain gauge and measured discharge data at Ribb watershed.

Different works have been attempted by other researchers in the evaluation of rainfall variability in Upper Blue Nile catchments including Ribb watershed using satellite rainfall (Haile et al., 2009) and CFSR data (Dile and Srinivasan, 2014). However, the

use of the selected satellite rainfall products for the assessment of water availability using the SWAT model has not been explored so far in Ribb watershed.

The results of this study are promised to provide the reliability of the selected satellite rainfall products relative to rain gauge data, the calibrated SWAT model and the quantified water balance components using two SRPs.

1.1. Statement of the problem

Nowadays, the impacts of climate change on water resource availability have become a headline issue for the global community. The effects of the climate change are alarming in all aspects as it is triggering hydrological extreme events and altering rainfall patterns. Wet regions are getting wetter and dry regions are getting drier. This affects the agricultural community of the developing countries including Ethiopia, where the livelihood of more than 85% of the populations is based on rain-fed agricultural produces. However, the spatiotemporal distribution of rainfall is generally variable. In relation to this, the Ethiopia is faced with a myriad of water related problems such as recurrent flood and drought especially in Ribb watershed. Thus, to alleviate these challenges, there have been routine information on local rainfall for reliable hydrological predictions and extreme managements. However, the availability of the ground measuring stations in Ribb watershed is very sparse. The limited ground measuring station would have problems, for instance missing records and inadequate area coverage that leads improper representation of spatiotemporal information of the rainfall pattern in many parts of the continent (Diro et al., 2009). In this case, for the better estimate of the localized rainfall in such kind of areas deploying satellite rainfall products might be valuable. In addition, sustainable water resources management can be achieved if there is a wide-ranging information on water availability coupled with quantification of the spatiotemporal dynamics of water balance variables (Wagner et al., 2009). However, water availability in Ribb watershed has not been yet examined using the selected satellite rainfall products as an input to the SWAT model. Therefore, this research analyzes the performance of satellite rainfall products and proposes their utility for examining the water availability in Ribb watershed.

1.2. Research questions

1. To what extent the selected satellite rainfall products agreed with gauged rainfall in Ribb watershed?
2. How the SWAT model streamflow simulation does perform over Ribb watershed?
3. How the prediction of water availability in terms of water balance components over Ribb watershed looks like using satellite rainfall data from 2000 to 2013?

1.3. Research objectives

The main objective of this research is to examine the application of satellite rainfall products for the assessment of water availability using a semi-distributed hydrological model Soil and Water Assessment Tool (SWAT) streamflow simulation for Ribb watershed.

The specific objectives of this research include:

1. To compare the satellite rainfall products against rain gauge data in Ribb watershed from 2000 to 2013

2. To evaluate the performance of Soil and Water Assessment Tool (SWAT) model using rain gauge and measured discharge data at Ribb watershed from 2000 to 2013

3. To appraise on the water availability of Ribb watershed in terms of water balance components through the calibrated SWAT model using satellite rainfall datasets from 2000 to 2013

1.4. Relevance of the study

This research focused on the application of satellite rainfall data for the assessment of water availability in Ribb watershed, Ethiopian highland. It provided a basis for the estimated water balance component in Ribb watershed and examined the performance of the satellite rainfall data compared to rain gauge data. It highlighted the use of satellite rainfall products as supplementary during the lack of data on the ground. The result of this research also provides pertinent information to land and water resources practitioners/ managers in Ribb watershed for the sustainable utilization of water resources and proper regional water managements.

1.5. Limitations of the study

This research is mainly focused on the direct application of the selected satellite rainfall products for the assessment of water availability without considering the issues of bias correction of satellite rainfall data. We examined the water availability of the Ribb watershed only with the SWAT model simulation of water balance components based on the spatial, discharge, meteorological and selected satellite rainfall datasets without having any other data that are crucial for water availability assessment for instance data on demand and supply sides of water in the watershed. Our comparison techniques also focused on the amount rainfall estimated by each satellite rainfall products on the monthly time step at the watershed scale without attempting at a different rainfall intensity. The rain detection capability of the selected satellite rainfall products is not also included in the comparison techniques of this research work.

1.6. Conceptual framework of the study

In this research, a detail conceptual framework is used to guide the study and to develop unique outcomes that can be used by the research community, and land and water resources managers/ practitioners.

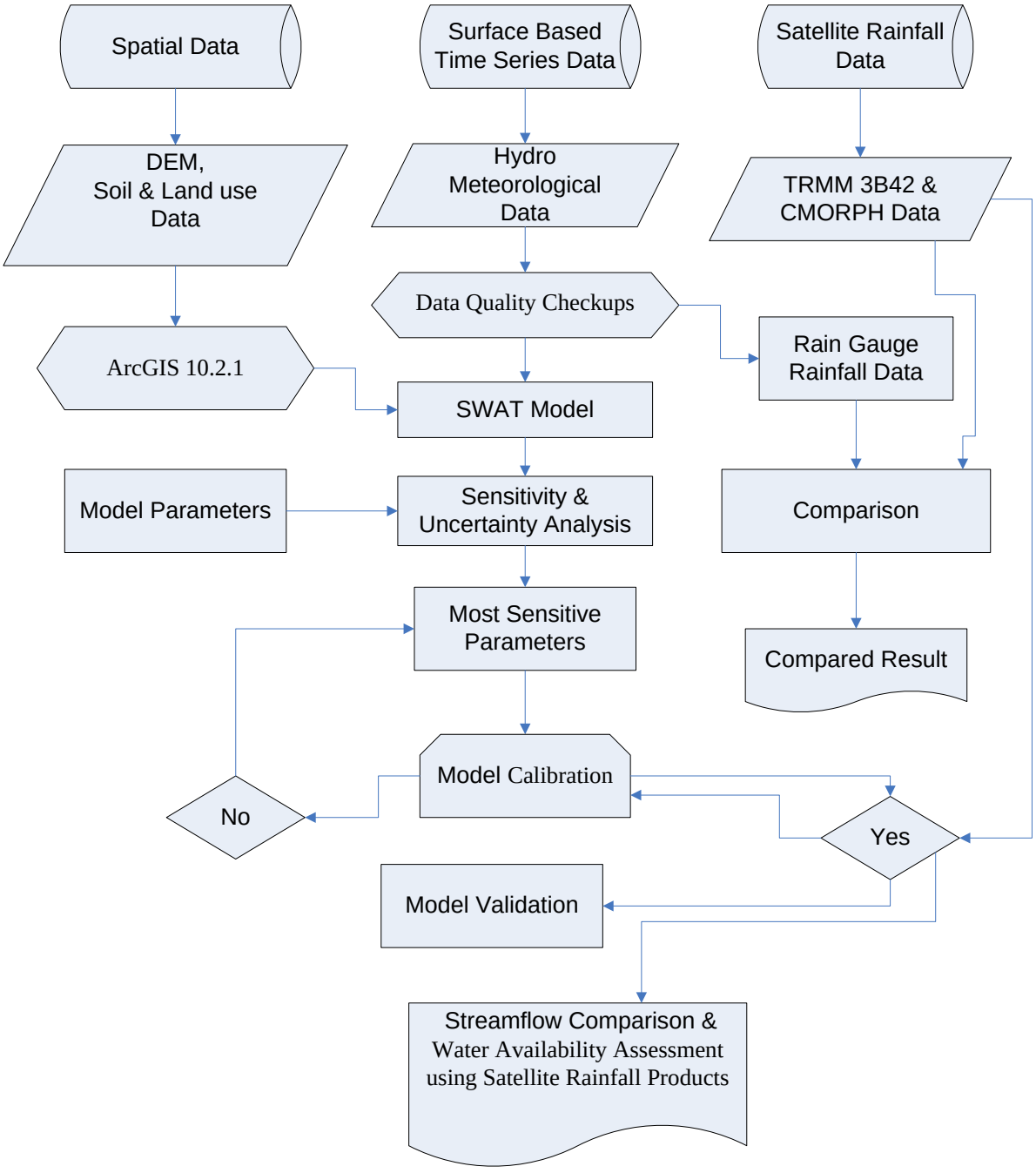

Figure 1.1 Conceptual framework of the study

CHAPTER TWO

2. Literature Review

2.1. Water availability and rainfall variability in Ethiopian highlands

Water availability can be described as the quantity of water hold in the soil profile that the plants can easily uptake from the surface (Tram et al., 2014). The amount of water available for plant and other uses is subjected to several factors such as the climatic, topographic, land use and land cover and practices. Thus, land, water interactions have to be continuously investigated in order to get updated information which is available in the watershed and important to support in decision-making processes (FAO, 2002).

Currently, the hydrological response of certain land parts can be dealt with the help of mathematical and hydrological models. The efforts through hydrological modeling can provide an insight about the local water balance and how a various management decisions effect on water availability and usage (Batchelor, 2013). Hydrological models have tremendous capability in the provision of representative water resources availability information. However, their applicability in developing country is mainly hindered by the absence of enough spatially distributed data (Grayson et al., 2002). Recently, the standard range-corrected radar products have shown tremendous capability of capturing the spatial variability of rainfall in the use of hydrological applications (Schuurmans and Bierkens, 2006). However, the availability of the precipitation measurement either rain gauge or radar is very scant in the Ethiopian highlands with that of Ribb watershed.

In developing country as well as Ethiopia the areal rainfall computations either at large basins or small watershed level are usually carried out through spatial interpolation approaches from the networks of surface based point measurements.

Often times in most part of the globe the interpolation approach is failing to represent the complete rainfall in the watershed because of an inoperative capability of rain gauge stations (Vrieling et al., 2010). Many of Ethiopian highland areas including Ribb watershed also has the same challenge due to its scant number of rain gauge stations. Hence, under such circumstances as well as for the attainments representative estimation of the rainfall in particular areas, the use of satellite rainfall estimate products could also be as an alternative to the surface based measurement.

Basically, highland watersheds are the major water sources for many countries and also for the largest rivers in the world too (Jain et al., 2010). Unless the proper watershed management interventions have been taken place, those highland watersheds would have been a threat e.g. by triggering soil loss on the upper parts and sedimentation for downstream areas. For instance, the annual fertile soil loss by water in the Ethiopian highlands is estimated around 1.9 billion (Selassie and Amede, 2014). On the downstream parts also, Roseires reservoir (Sudan) and Lake Nasser (Egypt) have lost 40% of their storage capacity due to sedimentation (Muala et al., 2014). Hence, to reduce such kind of burdens there have to be comprehensive investigations along with measurements of hydrological and climatic datasets.

Rainfall is a main climatic component that might exist in the form of fog, snow, and rain (Gebregiorgis and Hossain, 2013). Hereafter, rainfall can be used alternately with precipitation. It is major driver factors in the hydrological cycle and is the key means of water source for the watershed (Kidd and Levizzani, 2011). The rainfall characteristics is variable in both space and time that makes somehow difficult to measure it using the conventional surface based measurements.

The rainfall variability over mountainous and adjacent lake areas of lake Tana basin were examined by including Ribb watershed as part of this study (Haile et al., 2009). The authors carried out analysis using hourly rainfall data from a network of newly installed rain gauges, and cloud temperature indices from the Meteosat Second Generation (MSG–2) Spinning Enhanced Visible and Infrared Imager (SEVIRI) satellite sensor. The authors concluded that the rainfall variation in the sources of the Blue Nile river is influenced by elevation and distance from the lake.

2.2. Previous related works

There have been few studies which was investigated on the assessment of the performance of satellite-based rainfall products at different spatiotemporal scales.

The comparison of three high-resolution satellite rainfall products with rain gauge data over very complex topography in Ethiopia, nevertheless their analysis was restricted only to the mean annual time step and Ribb watershed was not included (Hirpa et al., 2010).

The evaluation of three high-resolution satellite rainfall products over Ethiopian river basins was carried out, but their comparisons were only limited for seasonal temporal scale, elevation and river basin (Romilly and Gebremichael, 2011).

Worqlul et al. (2014) comparison of rainfall estimations by TRMM 3B42, MPEG and CFSR with ground-observed data for the Lake Tana basin, including Ribb watershed. The authors applied point-to-grid and areal comparison methods on the monthly time step. In both cases of comparison, they obtained the TRMM 3B42 rainfall products performances were unsatisfactory.

Gebregiorgis et al. (2016) use of remote sensing based precipitation data from 3B42RT for flood frequency analysis in data-poor regions case of Blue Nile river basin, including the Ribb watershed. The authors concluded that application of the satellite rainfall data for flood frequency analysis is beneficial and capable in capturing the highest events.

The applicability of the national centers for Environmental prediction's climate forecast system Reanalysis (CFSR) climate data in modeling the hydrology of the region in Blue Nile River Basins (Dile and Srinivasan, 2014). The model simulation was conducted using both CFSR and conventional weather data without calibrations. They have found unsatisfactory model performance with both CFSR and conventional weather data for the Ribb and Megech rivers. The authors also highlighted that the poor performances of SWAT model over Ribb river, possibly errors in discharge data.

2.3. Satellite rainfall estimation and product descriptions

Satellite rainfall estimation algorithms uses two types of sensors. Geostationary satellites, which remain immobile relative to the Earth, use infrared channels to gather rainfall rates from cloud-top temperatures. They provided high resolution data, with continuous temporal coverage for any region. Polar-orbiting satellites use microwave channels which can provide better estimates of rainfall by monitoring the scattering of naturally emitted microwaves within clouds. However, as these satellites pass over a given location only once or twice a day, there are gaps in the time-series of data for any studied region.

The very basic idea within the high-resolution satellite rainfall estimations, algorithms have the merged information from the more accurate (but not frequent) microwave (MW) with the more frequent (but indirect) infrared (IR) for the sake of taking their complementary strengths (Bitew et al., 2012) .

The quality of satellite rainfall estimates is varying from one product to product and from one climatic region to region (Dinku et al., 2007; Duan et al., 2016). Therefore, exploring the applicability to their performance with some independent measurements is helpful for the product developers and end users.

The satellite rainfall estimates are readily available at high spatiotemporal resolutions and providing an optional representative estimate of rainfall variability in data scares and ungauged watershed (Sawunyama and Hughes, 2008). Among the bunch of satellite rainfall products which are readily available at the global scales TRMM 3B42 version 7 and CMORPH were used with a spatial and temporal resolution (0.25°x 0.25° and daily time step). The reason of selection satellite rainfall product was made based on their coincidence of the availability with rain gauge datasets. Their better spatial and daily temporal resolution for the relevance of the targeted hydrological model applications. The TMPA products exhibited good performances and offers quality of information, especially for the long term hydrological predictions (Mantas et al., 2015; Meng et al., 2014).

The TRMM is a collaborative mission between the National Aeronautics and Space Administration (NASA) and the Japan Aerospace Exploration Agency (JAXA) to detect the tropical and sub-tropical rainfall. The TRMM Multi-Satellite Precipitation Analysis (TMPA) algorithm provides the 3B42RT (near real time), 3B42 and the 3B43 products (Huffman et al., 2007).

TRMM 3B42

Tropical Rainfall Measuring Mission (TRMM) Multisatellite Precipitation Analysis (TMPA) algorithm forms the rainfall estimates by merging from microwave and infrared satellites as well as gauge analysis (Huffman et al., 2007). TRMM 3B42 product offers up to 3-hourly precipitation at a spatial resolution of 0.25° by 0.25° through the global coverage between 50° N–50° S from 1998 to present.

The TRMM 3B42 version 7 (post-real time) has an additional improvements over the TRMM rainfall products, owning to its adjustment using the Global Precipitation Climatology Centre (GPCC) monthly gauge analysis. It was accessed from the Goddard Earth Sciences Data and Information Services Center at http://mirador.gsfc.nasa.gov. There are two types of TRMM 3B42 product are available: Those are 3-hourly and daily accumulated products. The daily accumulated TRMM 3B42 version 7 product from the period 2000–2013 was taken for this research work.

CMORPH

CMORPH is developed with amalgamation of data derived from the United States Defense Meteorological Satellite Program satellites, and from the TRMM. It has coverage 60° N to 60° S and the data are available from January 1998 to date.

The CMORPH products are acquiring the rainfall estimates from MW data, then uses a motion vector from IR observations so as to derive a cloud motion field which enables to propagate high quality rainfall pixels (Joyce et al., 2004).

The passive microwave devices on board these satellites include the Advanced Microwave Sounding Unit-B (AMSU-B), the Special Sensor Microwave Imager

(SSM/I), and the TRMM Microwave Imager (TMI), respectively (Kimani et al., 2016).

2.4. SWAT model background

The SWAT (Soil and Water Assessment Tool) is a spatially distributed watershed scale and computationally efficient model this attributable to, its capability of simulating the effect of land management practices on the water in very large complex watershed under changing soil, land use and management issues over a long-time period (Breuer et al., 2009; Neitsch et al., 2011). SWAT takes intensive information of climatic, soil properties, topography, and land management practice of the watershed. SWAT model subdivides the watershed into various sub-watersheds, and then further sub-partitioned into hydrological response units (HRUs).

The simulation of watershed hydrology using the SWAT model is carried out into two main phases: the land phase and the routing phase. Whatever any problems studied in SWAT, the water balance is the central engine components of SWAT model which mimics the physical process involved throughout the watershed.

The following water balance equation is used to justify the land phase of the hydrological cycle in a watershed.

$$SW_f = SW + \sum_{i=1}^{t}\left(R_{day} - Q\,surface - ET - W - Qground\right) \quad \text{.....Equation 2.1}$$

SW_f, is the final soil water content in day (mm); SW is the initial soil water content in day (mm)

t is time in day (days), R_{day} daily precipitations (mm); $Q_{surface}$ surface runoff in day (mm), ET daily evapotranspiration (mm); W daily percolations (mm); Q_{ground} daily ground water flow (mm).

The land phases of hydrologic cycle are regulating the amount of the water, sediment and nutrients etc. which are loading into the main channel of each sub basins.

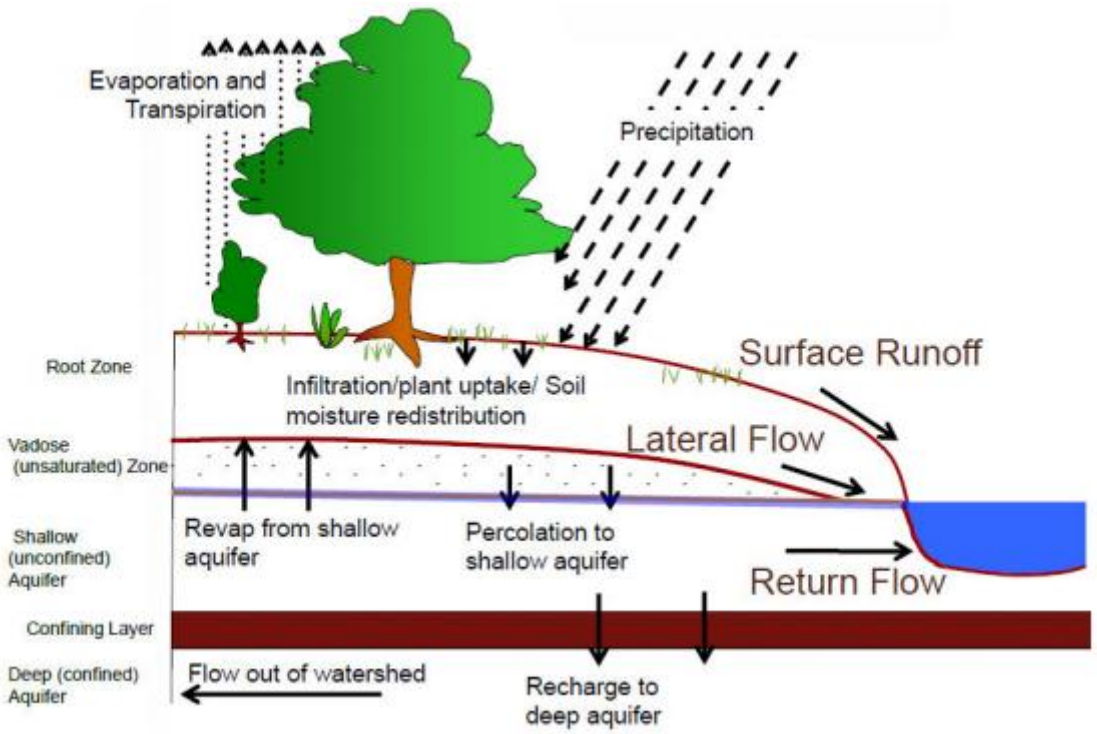

Sources (Neitsch et al., 2011)

Figure 2.1 Schematic representation of the hydrological cycle in the SWAT Model

2.4.1. Surface runoff

Surface runoff is initiated when the rainfall intensity is in excess of the infiltration rate. In the most of Ethiopian Blue Nile hill slope areas the runoff generation occurs when the soil saturates from degraded and shallow soils (Engda, 2009). SWAT simulates the watershed surface runoff at each HRU through either of the modified Soil conservation services (SCS) curve number method (USSCS, 1972) or the Green and Ampte infiltration method (Green and Ampt, 1911). The modified SCS curve number method is less data intensive than Green and Ampt infiltration method. Therefore, due to the availability of the hydro meteorological data at the daily scale we used SCS curve number method to calculate surface runoff depend on the area's land use, antecedent moisture content and hydrologic soil group for each HRU in the watershed, while Green and Ampt infiltration method needs rainfall data at sub daily scale that is not available on the ground.

The method is an empirical model and works based on the following equation:

$$Q_{surface} = \frac{(R_{day} + I_{day})^2}{R_{day} + I_{day} - S} \quad \text{……Equation 2.2}$$

$Q_{surface}$; the accumulated runoff or rainfall excess (mm)

R_{day}; the rainfall depth for the day (mm)

I_{day} ; the initial abstractions which includes surface storage, interception and infiltration

prior to runoff (mm)

S; the retention parameter (mm)

The retention parameter varies spatially because of changes in soils, land cover, management and slope and temporally due to changes in soil water content. The retention Parameter is computed as:

$$S = 25.4\left[\frac{1000}{CN} - 10\right] \quad \text{…..…… Equation 2.3}$$

Where: CN is the curve number for the day. The initial abstractions, I_{day}, is commonly approximated as 20% of S.

$$Q_{surface} = \frac{(R_{day} - 0.2S)^2}{R_{day} + 0.8S} \quad \text{……...…Equation 2.4}$$

Runoff will occur when R_{day} greater than I_{day}. For CN, detailed descriptions are found in (Neitsch et al., 2005).

2.4.2. Peak runoff rate

SWAT also computes the peak runoff rate at each HRU by using the modified rational formula indicated in the equation below.

$$Pr_f = \frac{Q\,surface * A * D_C}{3.6 * T_C} \quad \text{…… Equation 2.5}$$

Pr_f, The surface runoff rate ($\frac{m^3}{s}$)

D_C, the fraction of daily rainfall that occurs during the time of concentration

$Q_{surface}$, is the surface runoff (mm)

A, the sub-basin area (Km^2)

T_C, the time of concentration for the sub watershed (hour) which can be estimated using Manning's formula and,

3.6, is the conversion factor.

The value of D_C can be calculated in SWAT model:

$$D_C = 1 - e^{\left[2 * T_C - \ln(1 - u_{0.5})\right]} \quad \text{Equation 2.6}$$

$u_{0.5}$, is the fraction of daily rainfall falling with in half hour of the highest intensity.

And then, the dimensionless parameter runoff coefficient (C) is computed as:

$$C = \frac{Q_{surface}}{R_{day}} \quad \text{Equation 2.7}$$

Where, R_{day} is the daily rainfall (mm).

2.4.3. Channel routing

In the routing phase of the hydrologic cycle can be defined as the movement of water, nutrients and sediments through the stream network of the watershed to the outlet. It operates on the principles of Manning's formula for the computation of the average velocity and flow rate. The runoff is routed through the stream network using a variable storage coefficient method or the Muskingum routing method. The variable storage method applies continuity equation in routing the storage volume, however, the Muskingum routing method models the storage volume in a channel length as a combination of wedge and prism storages. The variable storage method was chosen for this study, owning of the available data and for the sake of getting total simulated

available water at the outlet of the watershed with respect to all modeling inputs of the watershed.

2.4.4. Evapotranspiration

The model computes evaporation from soils and plants separately as it has been explained by (Ritchie, 1972). The actual soil, water evaporation is predicted by using exponential functions of soil depth and water content. Plant transpiration is also computed through a linear function of potential evapotranspiration and leaf area index (Neitsch et al., 2002). Consequently, the SWAT model has three options for estimating potential evapotranspiration:

Penman Monteith (Monteith, 1965), Priestley-Taylor (Priestley and Taylor, 1972) and Hargreaves (Hargreaves and Samani, 1985). These methods require different type of climate variables: Penman Monteith method requires solar radiation, air temperature, relative humidity and wind speed; Priestley Taylor method requires solar radiation, air temperature and relative humidity; whereas Hargreaves method requires an air temperature only. We preferred the Penman Monteith for potential evapotranspiration estimation indicated below, this because of its better estimation of PET using the necessary climatic factors which have an influence in evapotranspiration (Neitsch et al., 2011).

$$\lambda E = \frac{\Delta * (Rs - G) + \frac{\rho a * Cp}{ra}(es - ea)}{\left(\Delta + \gamma\left(1 + \frac{rc}{ra}\right)\right)} \quad \text{..... Equation 2.8}$$

Δ The slope of the saturation vapor pressure vs. temperature curve [kPa °C^{-1}];

λE the latent heat flux density [MJ m^{-2} day^{-1}];

E the depth rate evaporation [mm day^{-1}];

Rs The solar radiation at the surface [MJ m^{-2} day^{-1}] which can be calculated using Angstrom formula;

G the heat flux density to the ground [MJ m^{-2} day^{-1}];

ρa Density of air [kg m^{-3}];

Cp the specific heat at constant pressure [MJ kg^{-1} °C^{-1}];

es the saturation vapor pressure of the air at some height above the surface [kPa];

ea the actual vapor pressure of the air [kPa];

γ The psychometric constant [kPa °C^{-1}];

rs the plant canopy resistance [s m^{-1}];

ra the diffusion resistance of the air layer [s m^{-1}];

λ Latent heat of vaporization, defined as the energy required to convert a mass of liquid water into vapor [MJ kg^{-1}] and ρw Density of water [kg m^{-3}];

2.4.5. Lateral flow

Lateral flow occurs when water move laterally in the soil profile that includes the upper two meters below the ground surface. The shallow aquifer contributes lateral flow to the main channel within the sub watershed. This water may easily uptake by plant or soil evaporation. The remain water will percolate out of the soil profile which becomes aquifer recharge. The lateral flow for each soil profile within by SWAT model is computed through kinematic storage principles and the equation is described as follows.

$$\text{Rlat} = 0.024\left(\frac{2 * S * Ks * \sin\theta}{\beta e * L}\right) \quad \text{Equation 2.9}$$

Where:

Rlat is lateral flow [mm/ day];

S is drainable volume of soil water [mm/day];

Ks is saturated hydraulic conductivity [mm/h];

θ is slope of the land surface;

βe is drainable porosity;

L is flow length [m].

2.4.6. Percolation

Percolation is the vertical flow of water to the soil profile till it joins with the water table. Normally it occurs when the water content in the pores of a soil exceeds its field capacity and the pores in the layer beneath are still not saturated. The subsequent percolation flow rate is then governed by the saturated conductivity of the soil layer. The volume of water available for percolation in the soil layer is computed in SWAT model as follows:

$SWly, gre = SWly - FCly$ if $SWly > FCly$ ……...…. Equation 2.10

$SWly, gre = 0;$ if $SWly \le FCly$ …… Equation 2.11

Where:

$SWly, gre$ the drainable water volume in the soil layer on a given day [mm]*;*

$SWly$ the water content of the soil layer on a given day [mm]*;*

$FCly$ the water content of the soil layer at the field capacity [mm].

2.4.7. Groundwater

Water penetrates into the underground storage mainly by infiltration and percolation. SWAT simulates the groundwater flow contribution to the total streamflow from a shallow aquifer storage that is recharged by the water percolated from the beneath of the root zone (Arnold et al., 1993). SWAT works with an exponential decay weighing function to account for the time delay in both aquifers recharge after the water exits the soil profile and given as follows:

$$Wrchrg,i = \left(1 - \exp\left(\frac{-1}{\delta gw}\right)\right) * Wseep + \exp\left(\frac{-1}{\delta gw}\right) * Wrchrg,i-1 \text{ ……. Equation 2.12}$$

Where:

$Wrchrg,i$ the amount or recharge entering the aquifers on day i [mm of water];

$Wseep$ the total amount of water exiting the bottom of the soil profile on day i [mm of water];

δgw the delay time or drainage time of the overlaying geologic formations [days];

$Wrchrg,i-1$ the amount or recharge entering the aquifers on day i-1 [mm of water];

The total amount of water leaving the bottom of the soil profile on day i is described as:

$Wseep = Wper,ly = n + Wcrk,btm$ ..... Equation 2.13

Where:

$Wper,ly = n$ the amount of water percolating out of the lowest layer, n in the soil profile on day i (mm);

$Wcrk,btm$ the amount of water flow past the lower boundary of the soil profile due to bypass flow on day i (mm).

SWAT divides the amount of recharge. The ratio of overall recharge is diverted from the shallow aquifer to the deep aquifer is due to percolation and given as:

$Wdeep = \phi deep * Wrchrg$ ..... Equation 2.14

Where:

$Wdeep$ an amount of water moving to the deep aquifer [mm];

$\phi deep$ an aquifer percolation coefficient [mm].

The quantity of recharge to the shallow aquifer and given as:

$Wrchrg,sh = Wrchrg - Wdeep$ .....Equation 2.15

Where:

$Wrchrg,sh$ the amount of recharge entering the shallow aquifer on day [mm].

The water balance of the shallow aquifer can be described as:

$$AQsh,i = Qsh_{,i-1} - Wrchrg,i - Qgw,i - Wrevap,i \quad \text{.....Equation 2.16}$$

Where:

$AQsh,i$ the amount of water stored in the shallow aquifer on day i;

$Qsh_{,i-1}$ the amount of water stored in the shallow aquifer on day $i-1$;

$Wrchrg,i$ the amount of water recharge entering into the shallow aquifer on day $i-1$;

Qgw,i the groundwater flow in to the main channel on day i;

$$Qgw,i = Qgw,_{i-1} - \exp(-\alpha gw * \Delta t) + Wrchrg * \left[1 - \exp(-\alpha gw * \Delta t)\right] \quad \text{.....Equation 2.17}$$

Qgw,i the groundwater flow into the main channel on day i;

αgw the base flow recession constant; Δt the time steps;

$Wrevap,i$ the amount of water moving into the soil profile and is lost to the atmosphere by soil evaporation or plant root uptake on day i and it is computed as:

$$Wrevap,\max = \beta rev \times PET \quad \text{if } AQsh > Rrevapmn \text{ ..... Equation 2.18}$$

Where:

$Wrevap,\max$ is the maximum amount of water moving into the soil zone [mm]; βrev is the revap coefficient; is PET the potential evapotranspiration [mm/day].

The water balance of the deep aquifer can be estimated as:

$$AQdp,i = Qdp_{,i-1} - Wdeep \quad \text{.....Equation 2.19}$$

Where: $AQdp,i$ the amount of water stored in the deep aquifer on day i [mm]; $Qdp_{,i-1}$ the amount of water stored in the deep aquifer on day $i-1$ [mm].

The amount of water flowing into the deep aquifer is not accounted in water balance budget of SWAT model.

CHAPTER THREE

3. Research Methodology

3.1. Location of Ribb watershed

Ribb watershed is situated at the northwestern part of Ethiopia with 11°42′36" to 12°13′48" N latitude and 37°43′12" to 38°14′24" E longitude in the Lake Tana basin in Amhara region. Rib River is one of the major tributaries of the Lake Tana. It originates from Guna Mountain in Farta district and crosses the main Bahir Dar to Gondar road at 10 km from Woreta Town. Based on the SWAT automatic watershed demarcation analysis, the total area of Ribb watershed is found about 1499.33 square kilometers. The topography of the watershed has varied from mountain area to hills areas including with flat areas. Ribb watershed has an elevation ranges from 1775 – 4077 meters as it is shown in the Figure 3.1.

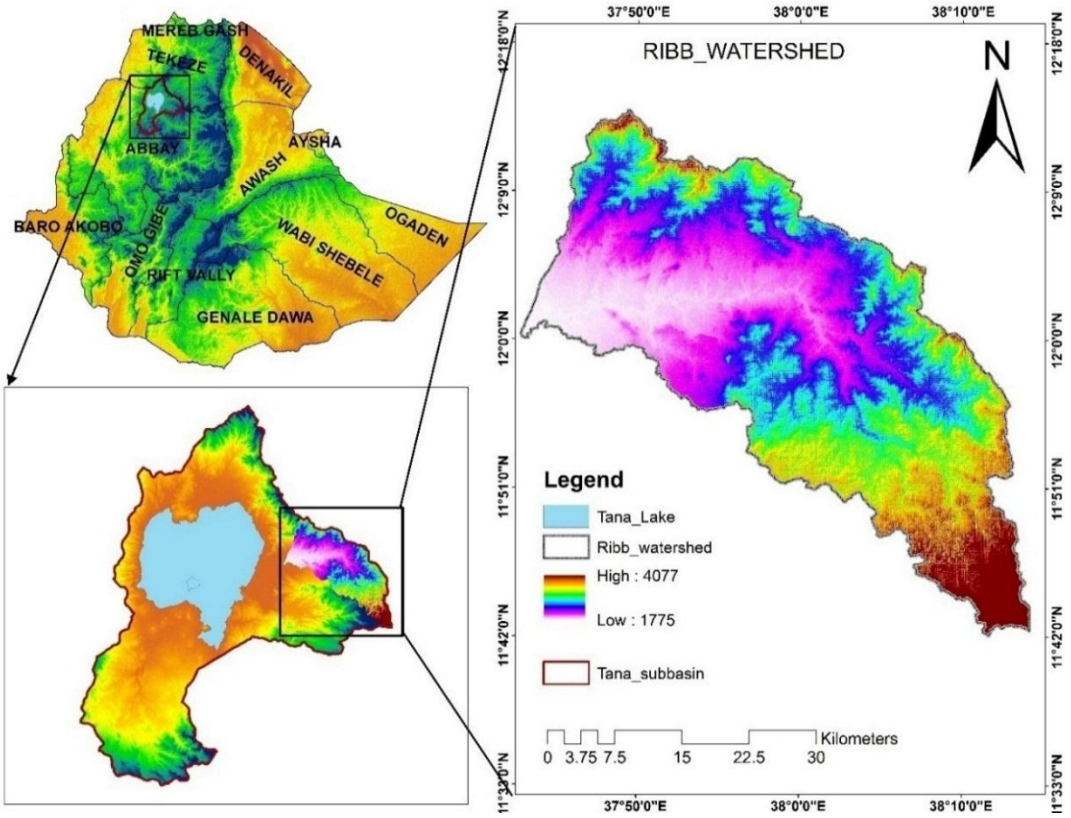

Figure 3.1 Location map of the study area

3.2. Climate and hydrology

The climate of Ethiopia is mainly influenced by ITCZ and there are three seasons commonly exhibited in Ethiopia. Those are: rainy season onset from June to cease at the end of September which contributes a large amount of rainfall (around 86 %) per annum for the country (Worqlul et al., 2014).

The average annual rainfall of the Ribb watershed is 1243.58 mm this is by using the rainfall data obtained from MoWIE (1998-2013) of four meteorological stations Woreta, Adiszemen, Amedber and Debretabor. Its average annual temperature maximum is 25.39°c and temperature minimum also 10.07 °c. Its average annual solar radiation is 19.56 MJ /m^2. The annual rainfall values also recorded at each station such as Adiszemen, Woreta, Amedber and Debretabor were 1322.79 mm,1108.15 mm, 1147.21 mm and 1256.58 mm, respectively.

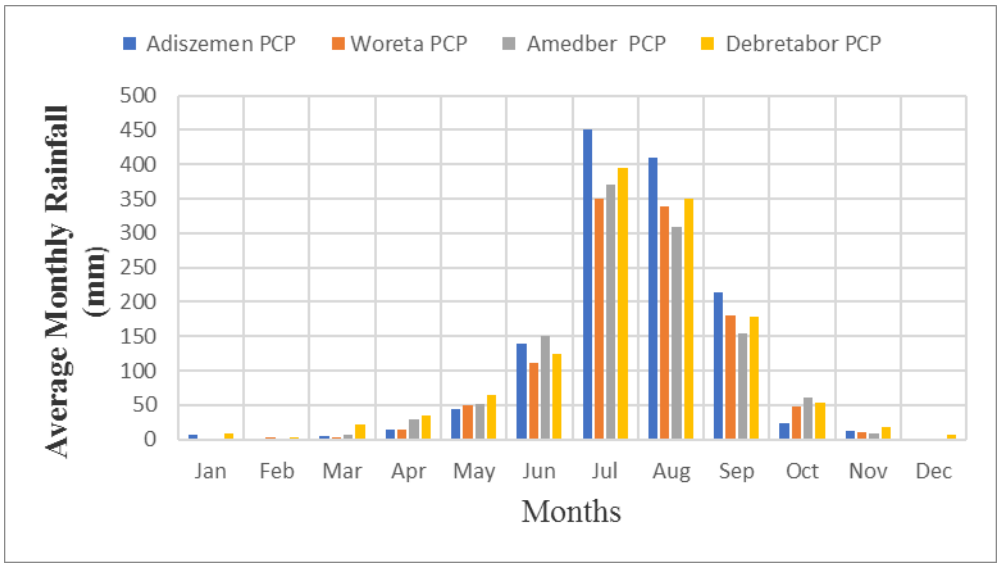

Figure 3.2 Average monthly rainfall rain gauge stations of Ribb watershed

The average monthly rainfall of watershed from 1988-2013 depicts the rainy and dry season patterns. As it can be seen Figure 3.2 rainfall rise from May to June and gradually descends starting from October.

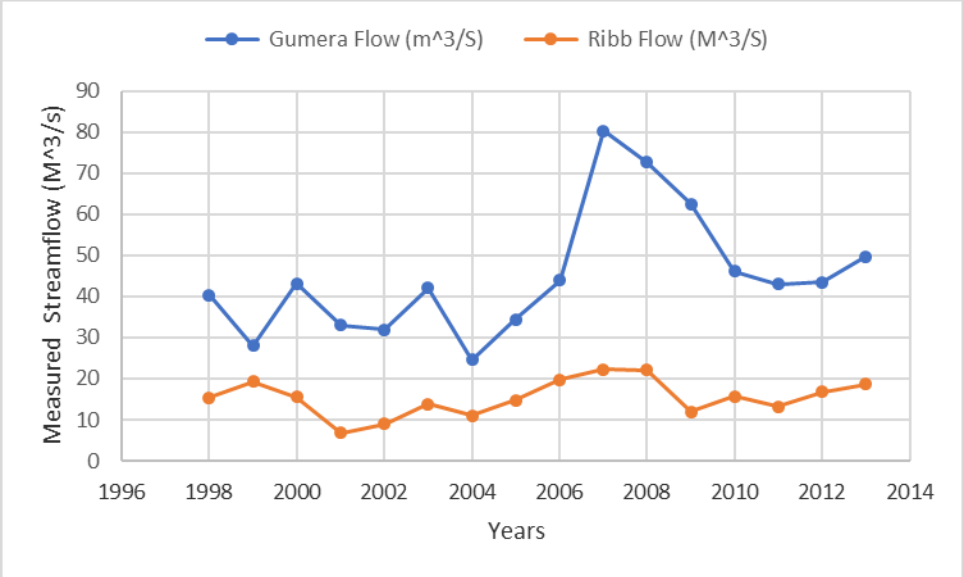

Figure 3.3 Average Annual measured discharge analysis from 1998 to 2013

The average annual measured streamflow values at Gumera and Ribb is 44.93 and 15.36 m^3/s, respectively. Hence, Ribb and Gumera discharge revealed the monomodal patterns which raised only in the rainy months.

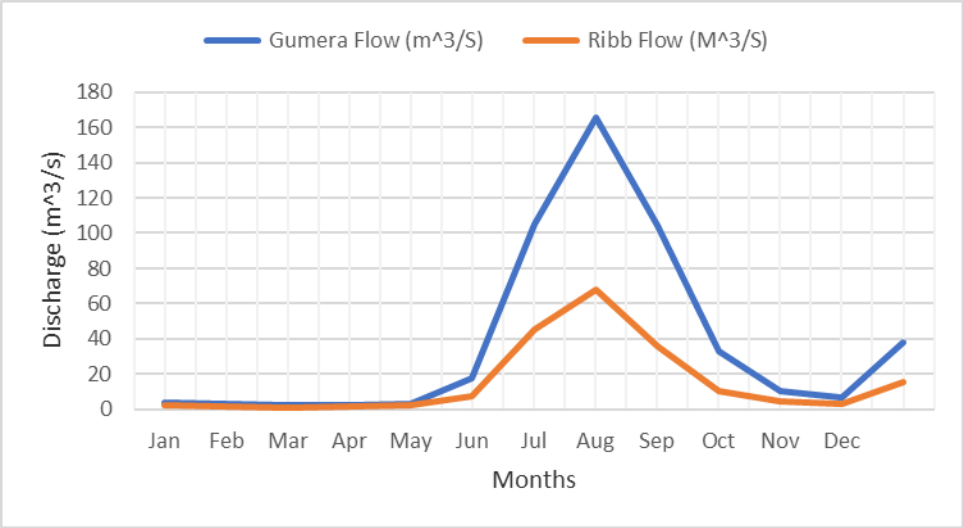

Figure 3.4 Average Monthly measured discharge analysis from 1998 to 2013

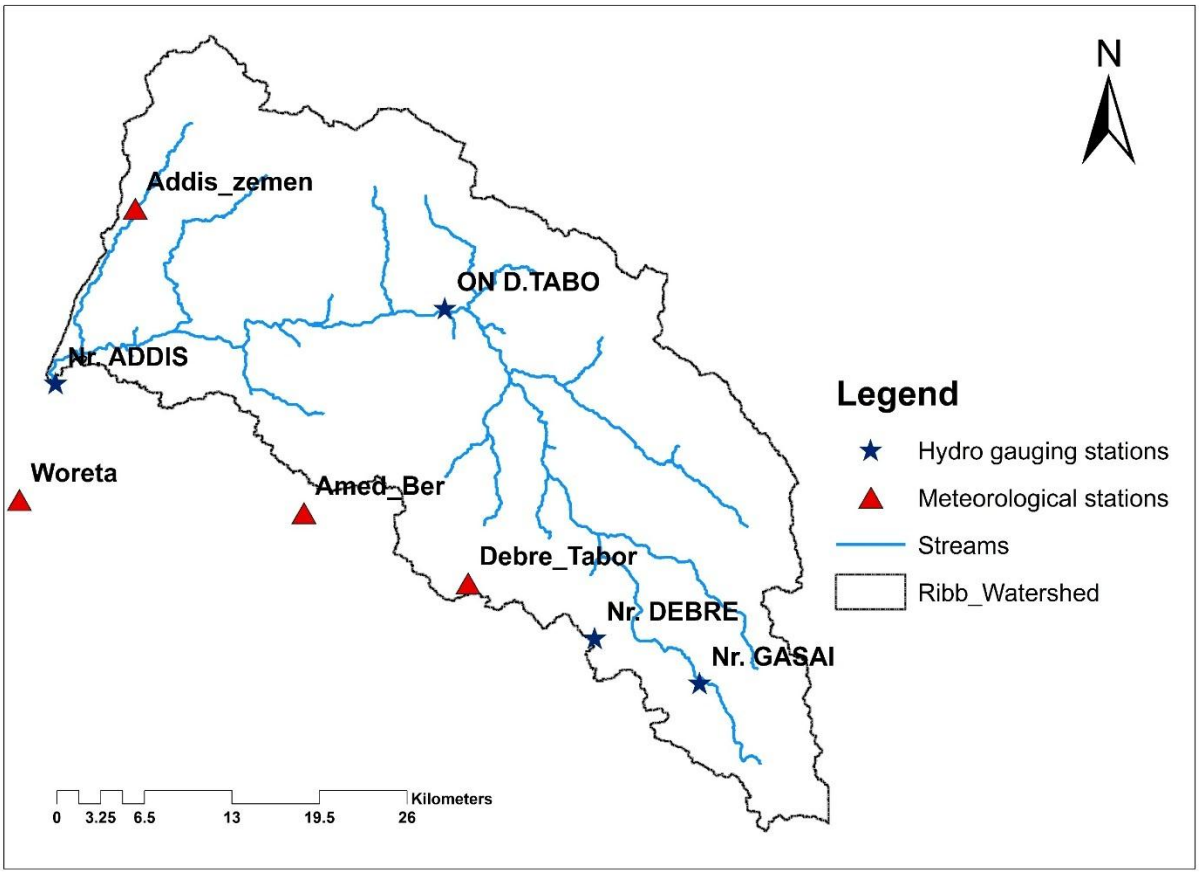

Figure 3.5 Hydro-meteorological stations of Ribb watershed

3.3. Soil types

The Ribb watershed has mainly covered with Eutric Vertisols, Haplic Luvisols, Eutric Leptosols, Chromic Luvisols, Haplic Nitisols and some part in urban soil type. The Ribb watershed is mainly dominated by Eutric Leptosols and which is followed by Chromic Luvisols soil types.

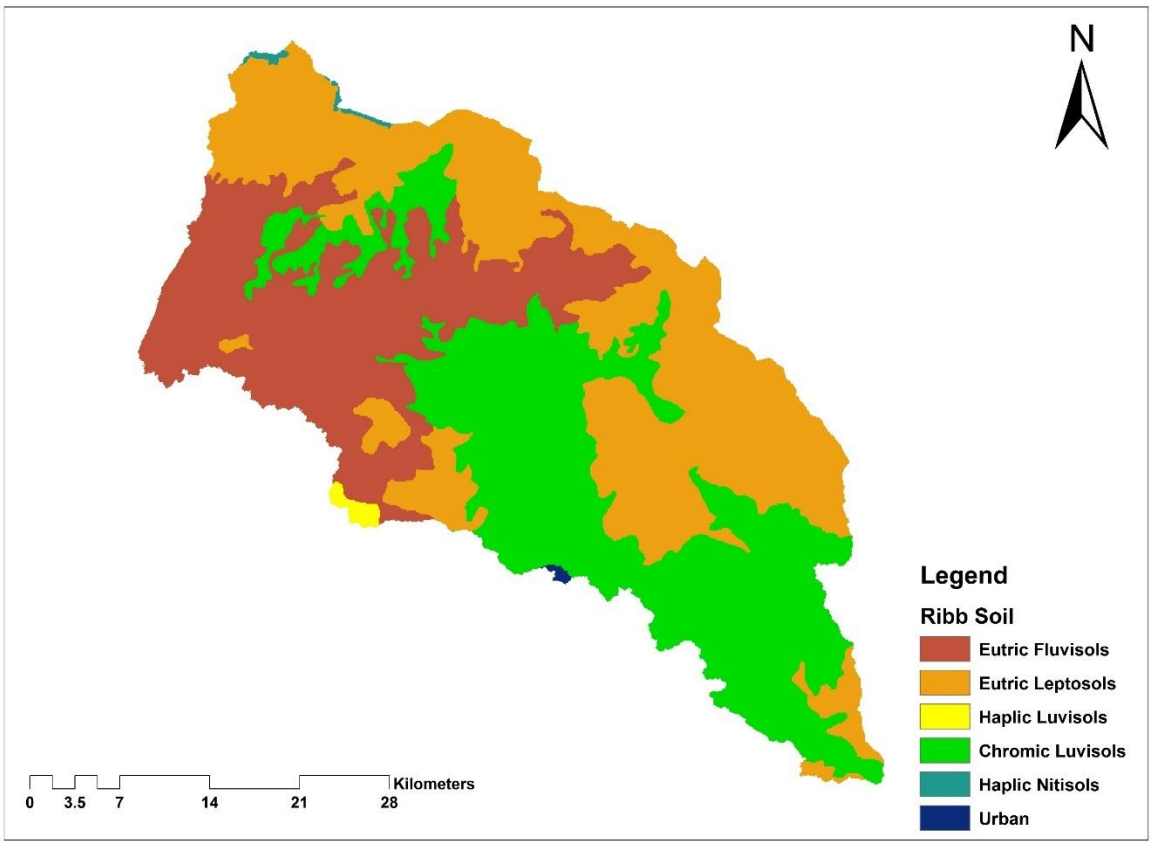

Figure 3.6. Types of soil in Ribb watershed

3.4. Land use/cover types

Land use and cover is the one factor that determines the overall status of hydrological components such as surface runoff, infiltration, Evaporation etc. of a certain region or watershed. As per the obtained land use/land cover data from MoWIE, Ribb the watershed land cover consists of dominantly cultivated (61.76%), moderately cultivated (24%), grassland (11.85%), afro alpine (1.5%), shrubland (0.21%), plantations (0.6%), urban (0.06%).

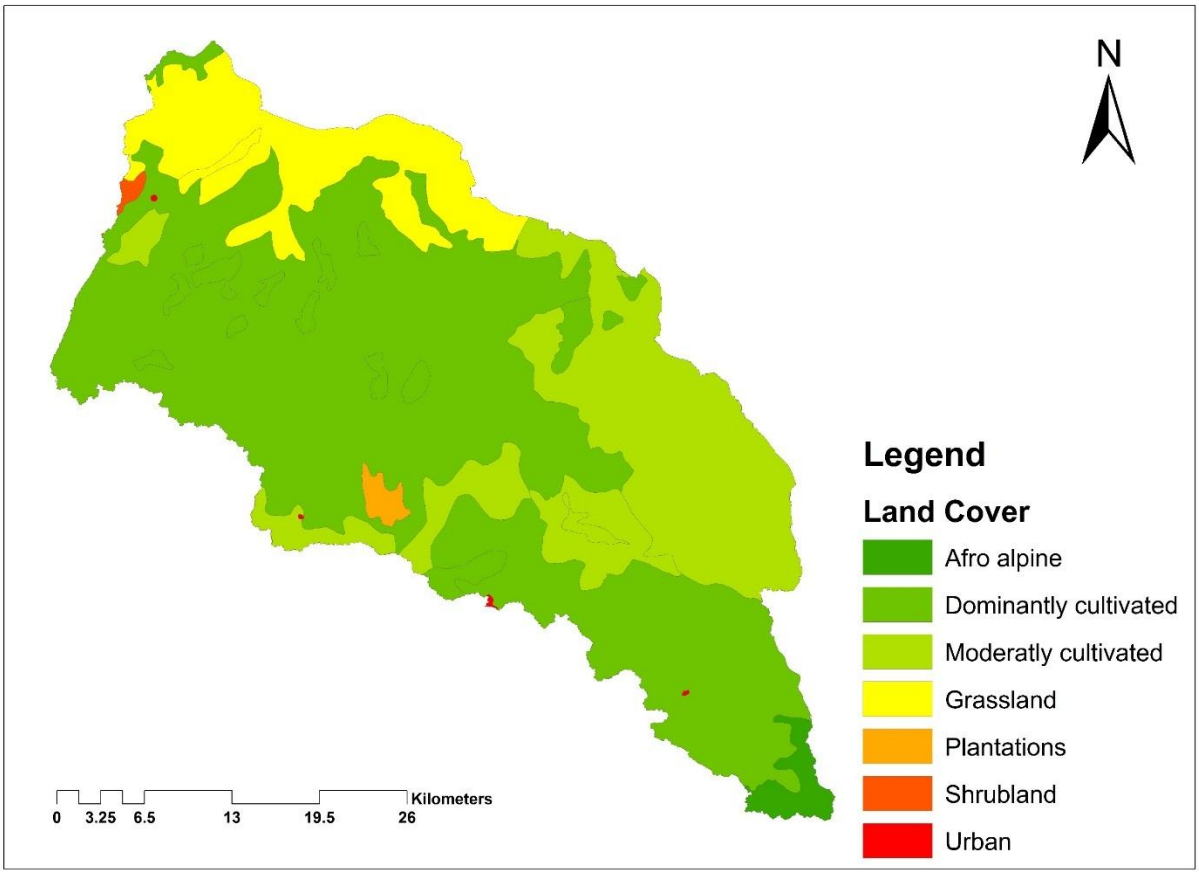

Figure 3.7. Land use and land cover of Ribb watershed

3.5. Data sources and quality control

In modeling and investigating the water availability in the Ribb watershed, the semi-distributed hydrological model (SWAT) is applied and which needs various datasets such as discharge, meteorological, DEM and soil. The data used for this study generally obtained from different institutions but, some of them were also downloaded from internet websites. The brief descriptions of each data are highlighted as follows.

3.5.1. Meteorological data

Daily meteorological data from the five climatic stations for the period of 1998-2013 were obtained from the National Meteorology Agency of Ethiopia (NMAE). Debretabor station has all daily meteorological elements which are rainfall, maximum and minimum temperature, wind speed, sunshine hour and relative humidity. It is a synoptic station (class I) since all climatic elements are measured every hour interval.

The rest of four stations which called ordinary stations (Class III) had only daily temperature maximum and minimum and rainfall. For the detailed data availability, descriptions are found in Table 3.1.

3.5.1.1. Solar radiation (Rs)

SWAT needs the solar radiation, which is not directly available in the meteorological stations. This is used to link with extraterrestrial radiation and relative sunshine period (Allen et al., 1998): Then we computed the solar radiation using the Angstrom formula as follows: when the daily sunshine hour is available on the synoptic station, we derived the solar radiation using the first equation. When it is missing, we derived the solar radiation using the second equation through the maximum and minimum temperature.

$$Rs = \left[as + bs\frac{n}{N} \right] Ra \quad \text{..... Equation 3.1}$$

Rs solar radiation [MJ m^{-2} day^{-1}];

n actual duration of sunshine [hour];

N maximum possible duration of sunshine or daylight hours [hour];

Ra extraterrestrial radiation [MJ m^{-2} day^{-1}];

$as + bs$ fraction of extraterrestrial radiation reaching the earth on clear days (n = N);

$\frac{n}{N}$ relative sunshine duration [-];

as regression constant, expressing the fraction of extraterrestrial radiation reaching the earth on overcast days (n = 0).

$$Rs = KRs\sqrt{T\max - T\min} * (Ra) \quad \text{.....Equation 3.2}$$

KRs an adjustment coefficient which is equals to 0.16 [-];

$T\max$ maximum air temperature [°c];

$T\min$ minimum air temperature [°c];

Table 3.1 The availability of all meteorological datasets used for this study

Stations Name	Coordinates (Decimal degree)		Elevation (meter)	Meteorological data					
				PCP	TMax	TMin	RH	ws	Sunhr
	Lat	Long							
Adiszemen	12.12	37.77	1940	Yes	Yes	Yes	NA	NA	NA
Amedber	11.91	37.89	2051	Yes	Yes	Yes	NA	NA	NA
Debretabor	11.87	38.00	2612	Yes	Yes	Yes	Yes	Yes	Yes
Enfranz	12.26	37.63	1937	Yes	Yes	Yes	NA	NA	NA
Woreta	11.92	37.70	1819	Yes	Yes	Yes	NA	NA	NA

Sources (NMAE) Note that: Year (1988-2013) and **NA** denotes not available.

3.5.2. Discharge data

Daily measured discharge data from 1998 to 2013 at Ribb and Gumera gauging stations was collected from the Ethiopian Ministry of Water Irrigation and Electricity. We used the Gumera gauging stations only for watershed descriptions. However, for modeling purposes, we used only the measured discharge data at a lower Ribb gauging station, which is the outlet of the Ribb Watershed. Two third of the measured discharge data was used for parameter sensitivity analysis and calibration of SWAT model parameters and the remainder data was used for validation of SWAT determined simulated results.

3.5.3. Spatial dataset

Soil data: soil data was collected from the different sources such as ministry of water irrigation and electricity of Ethiopia in the GIS department, but, it lacks soil parameters which are needed for SWAT model. Harmonized world soil data base (HWSD V 1.2) was also accessed from FAO website (http://www.fao.org/soils-portal/soil-survey/soil-maps-and-databases/harmonized-world-soil-database-v12/en/). Soil parameters such as bulk density, hydraulic conductivity and available water content were processed using Soil, Plant Atmosphere water (SPAW) Model.

Topography data: In hydrological modeling, relatively high resolution spatially distributed elevation data is indispensable for generating the hydrologic watershed

characteristics such as elevation, slope, stream network and watershed boundary. Digital Elevation Model (DEM) with the spatial resolutions of 30 meters by 30 meters was accessed from United States Geological Survey's (USGS's) National Elevation Dataset (https://earthexplorer.usgs.gov/).

Land use and land cover data: It was collected from ministry of water irrigation and electricity of Ethiopia in the GIS department.

All spatial datasets were projected using Arc tool box operation in ArcGIS 10.2.1 into Adindan UTM Zone 37° N which is the transverse Mercator parameters for Ethiopia.

3.5.4. Satellite rainfall products and data processing

The satellite rainfall products were downloaded from the internet website. The study period of satellite rainfall products was selected depending on the concurrent full availability of measured rainfall data for a period. CMOPRH and TRMM 3B42 were chosen as they are providing daily accumulated rainfall, which corresponds to the needs of SWAT model and collected rain gauge rainfall data. The previous study by (Dinku et al., 2007) on these products also exhibited their good performance in Ethiopia. The TRMM 3B42 version 7[1] data providers are Goddard Earth Sciences Data and Information Services Center and for CMOPRH[2] are Consiglio Nazionale delle Ricerche (CNR) or National Research Council. The data used for this study from both satellite rainfall products comprises from the year 2000-2013.

The satellite rainfall grids boxs were sub sited into the area of interest using ArcGIS 10.2.1 multi dimension tools by converting the netcdf file into raster layer. The grids which are laid the watershed were extracted by overlying the shapefile of the Ribb watershed. Then, using the selected grid latitude and longitude values, the rainfall value of each satellite rainfall products from each grid were accessed through MATLAB 2015. As it is shown in Figure 3.8 the Ribb watershed is laid over seven grid boxes with their latitude and longitude values ranges from (11.625, 38.125; 11.875, 38.125; 11.875, 37.625; 11.875, 37.875; 12.125, 37.625; 12.125, 37.875;

[1] https://disc.gsfc.nasa.gov/SSW/#keywords=TRMM_3B42_Daily with spatial 0.25°x0.25° and daily temporal resolution.
[2] https://wci.earth2observe.eu/portal/ with spatial 0.25°x0.25° and daily temporal resolution.

12.125, 38.125). Hence, the grid boxes with a spatial resolution of 0.25°× 0.25° latitude and longitude that covers the Ribb watershed is also illustrated in Figure 3.8.

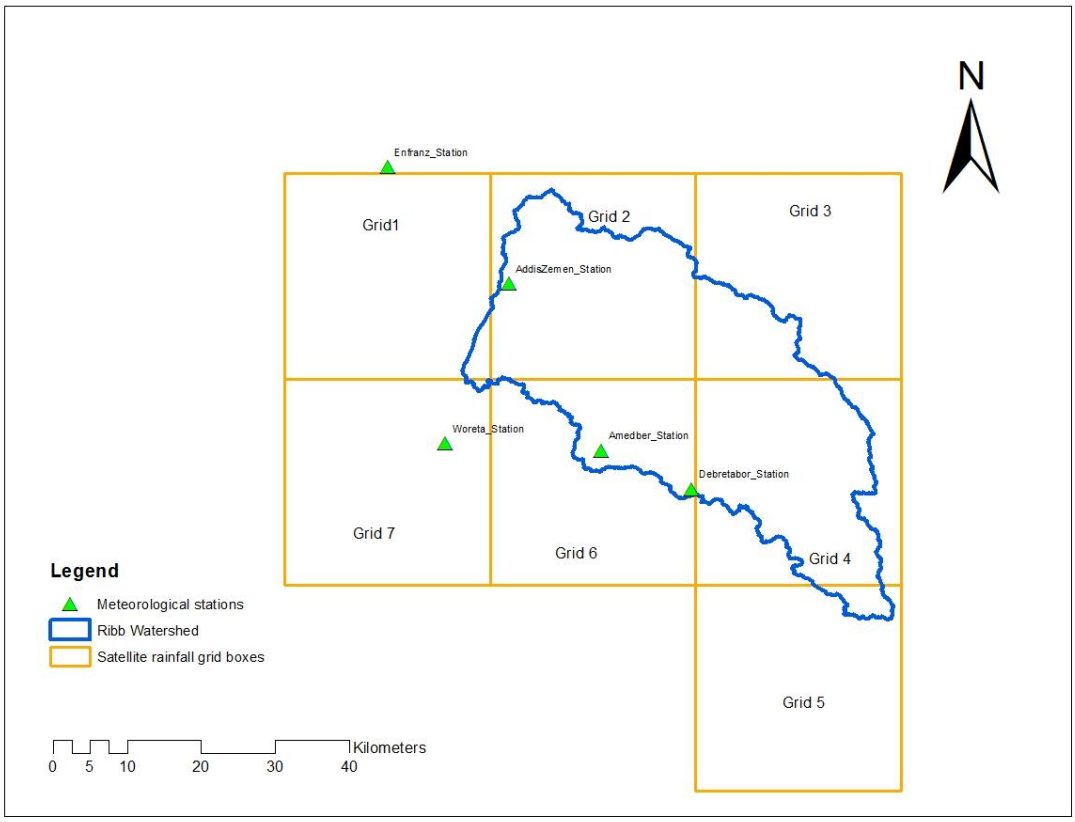

Figure 3.8 Location of satellite rainfall grid boxes covering the study area

3.5.5. Estimation of missing and outlier's detections

In most part of developing country as well as Ethiopia the hydro-meteorological data are usually exhibited gaps. This might happen due to several reasons such as the failures of the recording stations, shift of the stations, lack of regular observer in the stations etc. Hydrological modeling attempts for water resources planning and management are primarily hampered by such kind of gaps (Nkuna and Odiyo, 2011). Hence, before forcing these data into any hydrological modeling software, it has to be filled by the reasonable statistical filling method. For this study, after examining the gap in the time series data, the rainfall missing values were filled with the neighboring stations by the inverse distance weight method and the formula is indicated below. The weighting factors for the nearby stations are provided on the basis of their distance from the station under consideration to be filled. The assumption with this

method is that the closer stations are by far better correlated than those far away from the station under consideration. This method fills the missing values in a station under consideration from the nearby stations (Teegavarapu and Chandramouli, 2005).

$$P_{Comp,\,j} = \frac{\sum_{i=1}^{n_{Bas}} P_{i,\,j} / D_i^b}{\sum_{i=1}^{n_{Bas}} 1 / D_i^b} \quad \text{..... Equation 3.3}$$

Where:

$P_{Comp,\,j}$ Completed rainfall at the station under consideration at time j

$P_{i,\,j}$ Measured rainfall at the neighboring station i at time j

n_{Bas} Number of neighboring stations taken into consideration

D_i Distance between the station under consideration and the neighboring station i

b Power of distance D used for weighting rainfall values at each station and its attached value is 2.

Table 3.2 The missing percentage values of meteorological datasets

Station name	Meteorological data (% of missing)					
	PCP	TMax	TMin	RH	ws	Sunhr
Adiszemen	7.26	9.34	9.87	NA	NA	NA
Amedber	15.08	16.65	15.61	NA	NA	NA
Debretabor	0.44	0.46	1.15	31.47	10.11	50.63
Enfranz	9.96	9.43	9.96	NA	NA	NA
Woreta	0	3.52	2.58	NA	NA	NA

Sources (NMAE) & year from 1998-2013

For the measured discharge data, we never attempted to fill the missing discharge values, but, we only detected the outliers within the time series of the discharge datasets through visual analysis. Similar outlier detection was also employed for meteorological datasets.

Table 3.3 The missing percentage values of measured discharge data

Name of Gauging Stations	Coordinates (decimal degree)		Area (km^2)	Discharge data (% of missing)
	Latitude	Longitude		
Ribb	12: 0: 0 N	37:43: 0 E	1592	7.26
Gumera	11:50: 0 N	37:38: 0 E	1394	11.12

Sources (MoWIE) & year from 1998-2013

3.5.6. Consistency of meteorological stations

Before any analysis have been made from the hydro meteorological data, it has to pass through the homogeneity test. Normally, double mass curve analysis is a useful techniques for checking the homogeneity of rainfall and discharge data (WMO, 2011). The double mass curve is the graphical representation of accumulated rainfall data at a station under consideration against the average cumulative rainfall of neighboring stations for periods of 16 years (1998-2013). It was done after treating missing values at all stations.

As it is indicated in the Figure 4.2 the meteorological stations have no any significant break in the slope of the curves and this portrays that a consistency of rainfall data on the daily time series between the rain gauge stations. Hence those stations can be used for further comparison and hydrological modeling, analysis within the Ribb watershed.

We screened the daily rainfall data from the four rain gauge stations with a complete temporal coverage 2000-2013 and used for the comparison purpose with satellite rainfall products.

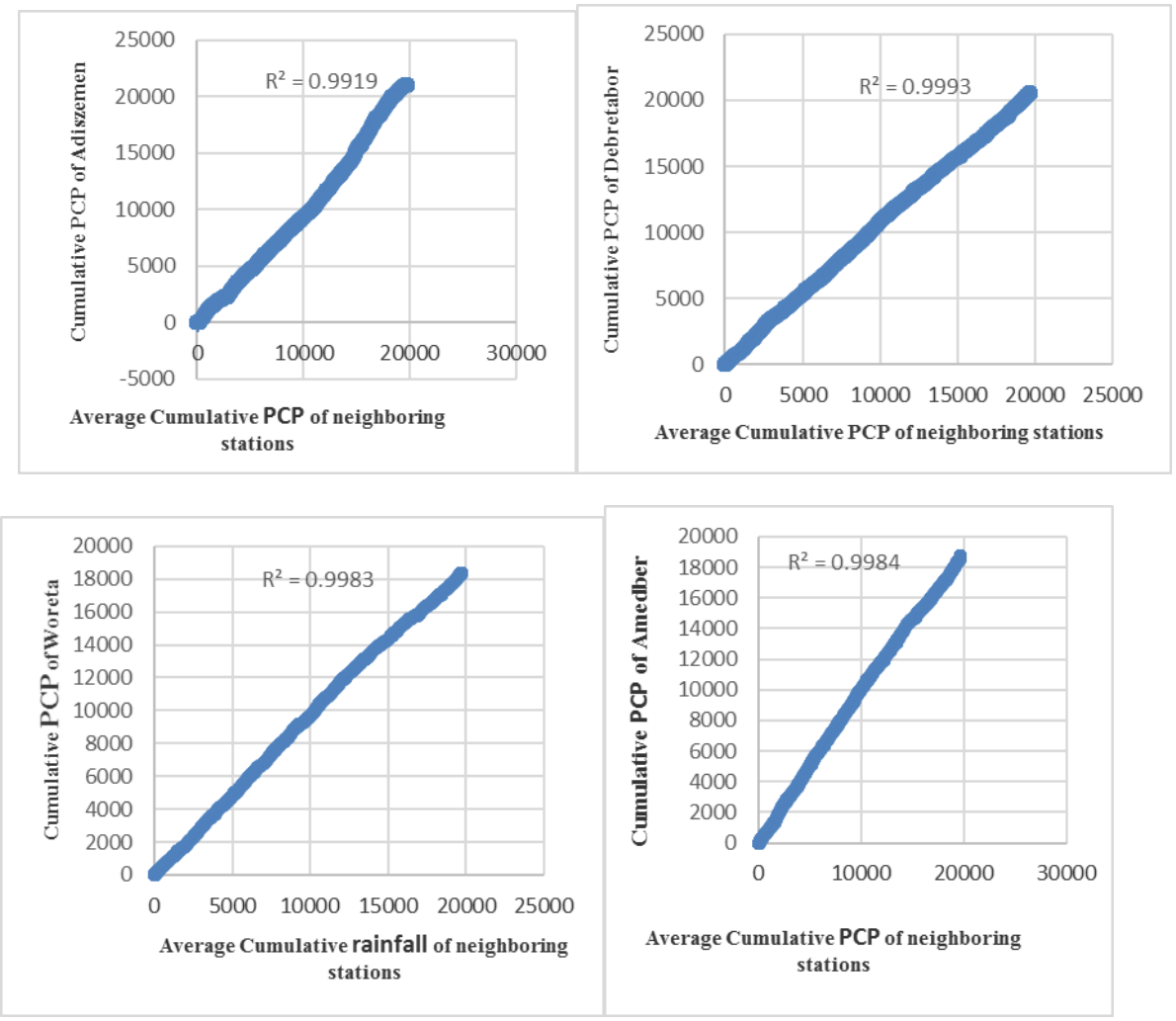

Figure 3.9 Double mass curve analysis for rainfall stations

3.5.7. Areal meteorological data computations

In order to have the overall idea about the rainfall falling on a given area of watershed, spatial interpolation is the common practices in many of the hydro-climatological studies. For this study, Thiessen polygon interpolation approach was employed to estimate the areal meteorological data. And then, we used this for describing the climate of watershed as well as for comparison of the satellite rainfall products against rain gauge station rainfall.

$$P_F = \frac{P_1 A_1 + P_2 A_2 + P_3 A_3 + \ldots + P_k A_k}{A_1 + A_2 + A_3 + \ldots + A_k} \quad \text{Equation 3.4}$$

Where P_F designated for the estimated average rainfall over the watershed, $P_1, P_2, P_3 \ldots\ldots P_k$ the measured rainfall at each station, $A_1, A_2, A_3 \ldots . A_k$ the areas of the Thiessen polygon which are created on the basis of those stations.

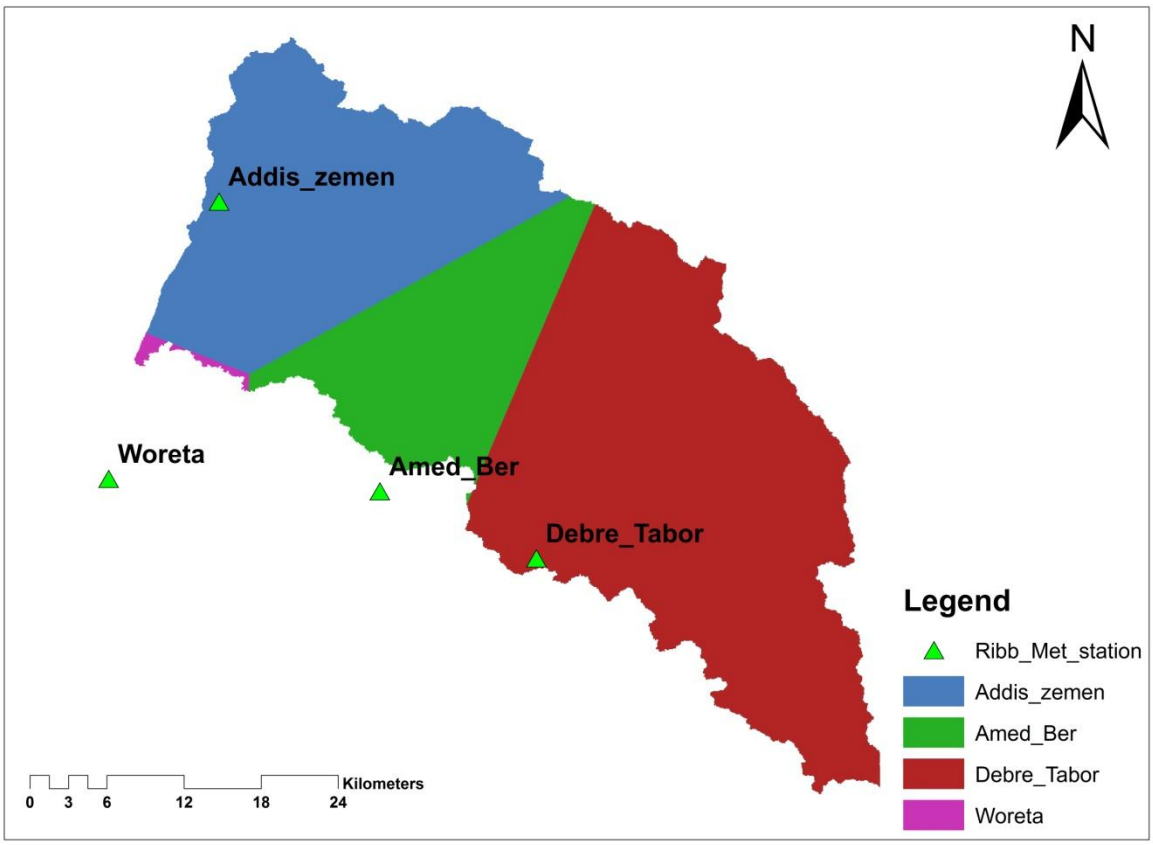

Figure 3.10 Thiessen polygon representation of Ribb watershed

CHAPTER Four

4. Methods of Comparison and Hydrological Modeling

In order to examine the application of satellite rainfall products for the assessment of water availability, the SWAT model was calibrated using rain gauge data and then the satellite data were forced on the calibrated model. Prior to the use of satellite rainfall products to for any hydrological applications, it is a good approach to assess their performance as compared to the ground based measurements (Jiang et al., 2012). Hence, we also compared the selected satellite rainfall products against the rain gauge rainfall data on the average monthly temporal scale and spatially watershed level. Even though some of the rain gauge stations had data starting from 1998, some of them also had gaps for some periods. Therefore, we selected the period of comparison from (1/1/2000-12/31/2013) to ensure an incessant coverage of data in line with satellite rainfall products datasets.

4.1. Methods of comparison of the satellite rainfall products

It is obvious that, the point measurements do not have the same spatial coverage as compared to gridded satellite rainfall. So, in order to compromise the scale discrepancy between them, the two sources of rainfall estimates were computed to give the same scale of area weighted rainfall over the entire watershed. To do so, there are a bunch of interpolation methods available such as inverse distance, kriging and Thiessen polygon method. Among these methods, Thiessen polygon interpolation was employed for areal rainfall computation owning to its simplicity and vigorousness (Grayson and Blöschl, 2001). This was performed in ArcGIS 10.2.1 Analysis Tools. The rainfall falling over the total watershed area from each satellite rainfall products and the rain gauge stations was computed through area weighted sum approach and the formulas are depicted in the equation 5.1 and 5.2. It provides quantitatively estimated areal rainfall over the entire watershed. Its intuition is to provide general information of rainfall the about the whole watershed on the basis of quantitatively estimated areal rainfall (Meng et al., 2014).

$$P_w = \sum_{i=1}^{n} P_i A_i \quad \text{.....Equation 4.1}$$

where, P_w is the total rainfall computed from each rain gauge stations at watershed scale, P_i is the rainfall value at each rain gauge stations i, A_i is the percentage of area for each rain gauge stations i and n, is the numbers of the rain gauge stations in this case we used four rain gauge stations.

$$S_w = \sum_{i=1}^{n} S_i A_i \quad \text{..... Equation 4.2}$$

where, S_w is the total rainfall computed from each satellite rainfall products at watershed scale, S_i is the satellite rainfall value at each grid boxes i, A_i is the percentage of area for each grid boxes i and n, is the numbers of the grid boxes in this case we used seven grid boxes.

We used graphical and different statistical measuring indices in order to compare the total rainfall computed from each satellite rainfall products relative to the total rainfall computed from each rain gauge station at watershed scale.

Some of the statistical measuring indices techniques used for this work are Pearson correlation coefficient, coefficients of determination (R^2), bias and root mean-square error (RMSE), percentage of root mean-square error (RMSE%). The choice of these commonly used statistical measuring indices is taken deliberately in order to compare the result with the other findings (Mantas et al., 2015).

I. Pearson correlation coefficient (PCC) is used to assess the scale of agreement that reflects the level of linear correlation between the satellite and rain gauge rainfall data. Its value ranges from -1 to +1. Many researchers worked on the evaluation of the satellite rainfall products including TRMM and CMORPH rainfall products also used the Pearson correlation coefficient as the standard measuring statistical indices (Dembélé and Zwart, 2016; Mantas et al., 2015; Ochoa et al., 2014; Yang et al., 2013).

$$PCC = \frac{\sum_{i=1}^{N}\left[(Si-\overline{S})*(Ri-\overline{R})\right]}{\sqrt{\sum_{i=1}^{N}(Si-\overline{S})^2}*\sqrt{\sum_{i=1}^{N}(Ri-\overline{R})^2}} \quad \text{..... Equation 4.3}$$

Where: S_i designated for the satellite rainfall estimate in a month i and R_i is represented for the rain gauge rainfall, N denotes number of temporal time steps rainfall in the analysis. $\overline{R}$ and $\overline{S}$ are the average value of the rain gauge and satellite rainfall data, respectively.

II. Coefficients of determination (R^2) is the ratio of variability in the rain gauge rainfall data showed up by the satellite rainfall data sources (Liu et al., 2015). One is its perfect value.

$$R^2 = \left[\frac{\sum_{i=1}^{N}\left[(Si-\overline{S})*(Ri-\overline{R})\right]}{\sqrt{\sum_{i=1}^{N}(Si-\overline{S})^2}*\sqrt{\sum_{i=1}^{N}(Ri-\overline{R})^2}}\right]^2 \quad \text{..... Equation 4.4}$$

III. Bias reveals the level of over and under estimation of satellite rainfall as compared to the measured rainfall value (Duan et al., 2012).

$$Bias = \frac{\sum_{i=1}^{N}S_i - \sum_{i=1}^{N}R_i}{\sum_{i=1}^{N}R_i} * 100 \quad \text{..... .....Equation 4.5}$$

Where: its value ranges from negative ∞ to positive ∞ but, zero is perfect value.

IV. Root mean-square error (RMSE) is the difference between satellite rainfall and rain gauge rainfall values which gives the average magnitude of the approximation errors (Dembélé and Zwart, 2016). It is used to examine spatial patterns of the rainfall. Its value ranges from 0 to positive ∞ and perfect value is zero.

$$RMSE = \sqrt{\frac{1}{N}\sum_{i=1}^{N}\left(X - \overline{X}\right)^2} \quad \text{..... Equation 4.6}$$

Where: $X = (Si - Ri)$ for monthly timestep, $\overline{X}$ = The mean of X at monthly timestep

V. Percentage of root mean-square error (RMSE %) is the ratio of RMSE to the average rain gauge rainfall used to assess the reliability of the satellite rainfall. Zero is its perfect value.

$$RMSE\% = \frac{RMSE}{\overline{R}} \quad \text{..... Equation 4.7}$$

Based on the average monthly rainfall values, we also looked at the amount of the rainfall estimated by each rainfall data source for each season.

4.2. Arc SWAT model inputs and modeling process

The Arc GIS 10.2.1 with Arc SWAT 2012 interface was used to setup and parametrize the model for the Ribb watershed. The daily weather data, such as rainfall, maximum and minimum temperature, solar radiation, relative humidity and wind speed. These are the major determinant inputs along with the listed spatial datasets for estimating the water balance components of Ribb watershed by SWAT model.

4.2.1. Watershed delineation

The watershed delineation was done from DEM as the main initial input using SWAT's built-in automatic watershed delineation tool. DEM was hydrologically corrected before importing into the defined SWAT Project. This includes projection, filing sinks were done in ArcGIS 10.2.1 Arc tool box and the rest was completed in Arc SWAT. After loading the DEM, manual delineation was made and stream network was generated. And then, the final watershed boundary was delimited by locating lower Ribb discharge gauging station as an outlet point of the watershed to the SWAT's built-in automatic watershed delineation tool. Herein, DEM is the most important input data used to derive the hydrological parameters of the watershed such as slope, flow accumulation, flow direction, and stream network out of it and which are pretty much useful in the subsequent modeling process. In addition to this, it

provides the overall land surfaces alignments in general. After the watershed delineation has been made, 25 sub watersheds were generated and total area coverage of the Ribb watershed is obtained as 1499.33 km^2.

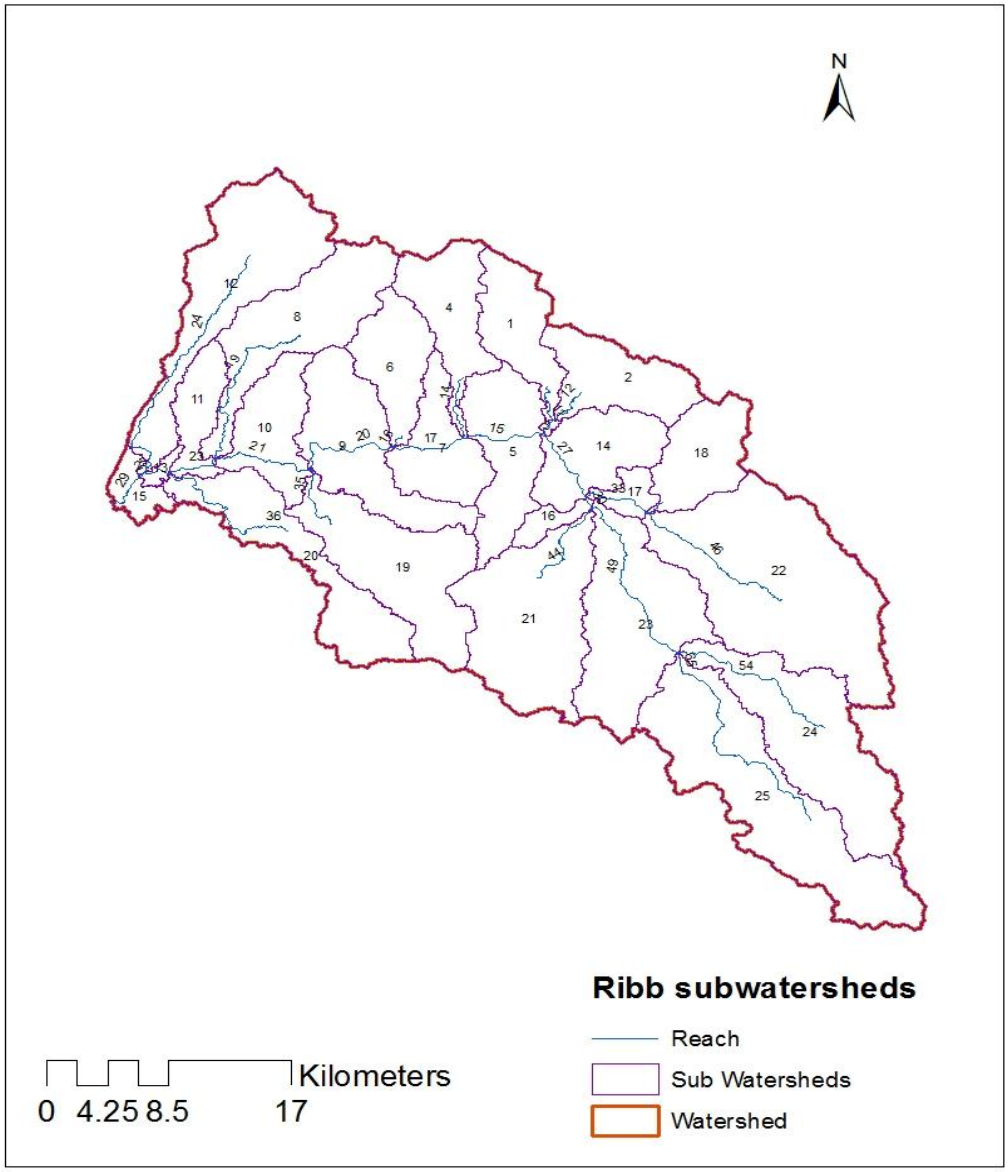

Sources (SWAT watershed delineation)

Figure 4.1 Number of sub watersheds generated using SWAT model

4.2.2. Hydrologic response unit analysis

Hydrological Response Units (HRUs) are the smallest units of the hydrological features that have unique land use, soil and slope combinations within the sub watershed. It is used to show the differences in evapotranspiration and other hydrological conditions under the various soils, slopes and land use and land covers. The runoff is computed distinctly for each HRU and then routed to attain the total runoff from the watershed.

HRU definition was done by using HRU analysis tools which desires LULC, soil and slope data. In order to account the spatial variability of the hydrological process, those data were prepared in gridded format and uploaded into The SWAT database. In case of the soil data, its physical and chemical properties of the parameters were updated in the SWAT soil database using FAO, Harmonized World Soil Database (HWSD). The types of major soil used in SWAT model are presented in (Table 4.1).

Table 4.1 Major soil types used for this study

Soil Types	SWAT Code	Texture	Area Coverage (% watershed)
Eutric Fluvisols	FLe	Loam	26.55
Eutric Leptosols	LPe	Loam	37.81
Chromic Luvisols	LVx	Clay Loam	35.12
Haplic Luvisols	LVh	Loam	0.42
Urban	UR	poor	0.1

We used the land use and land cover data from MoWIE for the SWAT model. The reclassification was made on the land use and land cover data as per the Arc SWAT 2012 land use database format. This was carried out on the basis of the previous research work, site reconnaissance data and use of background knowledge about the study area. The types of land use and land cover data used for SWAT model is presented in (Table 4.2). The predominant soil and LULC data were taken in each sub watershed. This an important process so as to alleviate the influence of soil and LULC which varies across the watershed and reducing the computational time of the model. Finally, an overlay operation was automatically performed that highlighted the distribution of LULC and soil all over the watershed.

Table 4.2 Land use and land cover types used in SWAT model

LULC Types	Swat Code	Area Coverage (% watershed)
Agricultural Land	AGRL	61.73
Grassland	GRAS	13.52
Dryland Cropland & Pasture	CRDY	23.98
Sylvicultural	FOEB	0.6
Urban	URMD	0.17

Ribb watershed has undulating topography and its slope acutely vary from one place to the other place. It is clear that, slope has a potential effect on the velocity of runoff initiations. So, we classified the watershed land features into five distinct slope classes using DEM which are used for taking care of the runoff regime at different level of land features. Their level of details of slope classes is presented in (Table 4.3). The multiple HRUs definition was made within each sub watershed by providing the defined values for each input. Therefore, we provided the threshold value 0% for LULC, 10% for soil and 10% slope for each sub watershed. And then, 309 HRU were created for the 25 sub-watersheds of the Ribb watershed.

Table 4.3 Slope classes used for SWAT model

Slope class (%)	Swat Code	Area Coverage (% watershed)
0-5	0-5	6.69
5-10	5-10	18.53
10-20	10-20	33.04
20-25	20-25	8.34
> 25	25-9999	33.39

4.2.3. Importing weather data

The daily weather data, such as rainfall, maximum and minimum temperature, solar radiation, relative humidity and wind speed are used by the SWAT model so as to drive hydrological balance compartments. The dew-point temperature is prepared with help of dew02.exe program using daily maximum and minimum temperature data (Liersch, 2003). The statistical parameters which are needed by the weather generator

of the SWAT model were computed from the daily rainfall data of the synoptic station (i.e. Debretabor) by helps of pcpSTAT.exe application (Liersch, 2003). Hence, these daily rainfall, maximum and minimum temperature along with their corresponding locations are prepared in database format (dbf) and linked with the model through weather data input wizards. For all simulations, Debretabor weather station data was served as weather generator.

4.2.4. Sensitivity and uncertainty analysis

Sensitivity analysis used to look at the relative changes of the model outputs in relation to the changing of model parameters. The capability of the hydrological model to reasonably simulate the streamflow as a result of different model inputs is evaluated through sensitivity analysis, model calibration, and model validation. It has to be passed through a scrutinized process of calibration tests and uncertainty analysis. Especially in physically based distributed models like SWAT mounts several factors and parameters for the simulation of watershed response to the dynamic process of the hydrological cycle. Undertaking the manual calibration under such circumstance is cumbersome and time-consuming activity.

Hence, the parameter sensitivity and uncertainty analysis were performed on a monthly time step through the auto-calibration and sensitivity analysis tool so called SWAT CUP which uses the Latin hypercube one-factor-at-a-time (LH-OAT) method. LH-OAT has blending global and local sensitivity analysis methods along with provision of parameter ranking on the basis of their importance (Sun and Ren, 2013). A Global Sensitivity Analysis (GSA) was done after 500 simulations on the 8 parameters comprised in the calibration process. GSA is initiated by SUFI-2 in SWAT CUP and can be made after one iteration.

SWAT CUP uses different algorithms for the sensitivity and uncertainty analysis. Some of them are Sequential Uncertainty Fitting version 2 (SUFI-2), Generalized Likelihood Uncertainty Estimation (GLUE) and Parameter Solution (PARASOL). We preferred SUFI-2 for sensitivity analysis and quantifying the model uncertainty. This is due to its capability of considering all the possible uncertainties (parameter, conceptual model, input, etc.) on the parameters ranges as the model goes in an

iterative process to catch up most of the observed data within the 95 percent prediction uncertainty (Abbaspour et al., 2009). The two statistical measuring indices which are ‘‘P-factor’’ and ‘‘R-factor’’ were used to evaluate the model predictive uncertainty (Abbaspour et al., 2004). Hence, we used a P-factor and R-factor for the quantification of uncertainty and it is calculated as follows:

$$\text{P - factor} = \frac{1}{n}\sum_{fj}^{n}\left(g^{y}_{fi,97.5\%} - g^{y}_{fi,2.5\%}\right) \quad \text{..... Equation 4.8}$$

$$\text{R - factor} = \frac{P-factor}{\delta Obs} \quad \text{..... Equation 4.9}$$

$g^{y}_{fi,97.5\%}$, $g^{y}_{fi,2.5\%}$ are designated the upper and lower boundaries of the 95PPU, and δ_{Obs} is the standard deviation of the observed data.

The goal of parameter sensitivity analysis is to minimize the estimated number of parameters which enhances the model efficiency by reducing the computational time required for model calibration. Sensitivity analysis was done before calibration has been made. This used for reducing uncertainty and identifying the most sensitive parameters which could be used in the subsequent modeling process. The impacts of model parameters also ranked depending on their degree of influence on model outputs and assessed by GSA values (t-stat and P-value).

The monthly SWAT simulated outputs were imported into SWAT CUP tools for sensitivity analysis. We took 19 SWAT model parameters as it can be seen in (Table 4.4) from the previous studies conducted in Upper Blue Nile Basins and Ribb watershed which could have a potential impact on the water balance and flow regimes of the Ribb watershed (Alemu, 2011; Girma, 2013; Setegn et al., 2008; Taffese, 2011; Tensay, 2011). We forced all model parameters into an automatic SWAT CUP tool for the sake of reducing the modeler’s bias and the numbers of calibration parameters (Bitew et al., 2012).

At the initial stage, we executed the SWAT CUP to run with the 500 iterations for each 19 SWAT model parameters from the years 2000-2009, the reaction of the highest sensitive parameters was identified. The choices of SWAT model parameter values were adopted from the SWAT user’s manual (Neitsch et al., 2002).

Table 4.4 Model parameters and their values range used for sensitivity analysis

S. N	Parameters	Descriptions of model parameter	Lower bound value	Upper bound value
1	r__CN2.mgt	SCS runoff curve number	-0.25	0.25
2	v__ALPHA_BF.gw	Baseflow alpha factor (days)	0	1
3	v__GW_DELAY.gw	Groundwater delay (days)	0	500
4	v__GWQMN.gw	Threshold depth of water in the shallow aquifer required for return flow to occur (mm)	0	5000
5	v__GW_REVAP.gw	Groundwater "revap" coefficient	0.02	0.2
6	v__REVAPMN.gw	Threshold depth of water in the shallow aquifer for "revap" to occur (mm)	0	1
7	v__RCHRG_DP.gw	Deep aquifer percolation fraction	0	1
8	r__SOL_AWC().sol	Available water capacity of the soil layer	-0.25	0.25
9	r__SOL_K().sol	Saturated hydraulic conductivity	-0.25	0.25
10	r__SOL_ALB().sol	Moist soil albedo	-0.25	0.25
11	v__CH_N2.rte	Manning's "n" value for the main channel	-0.01	0.3
12	v__ALPHA_BNK.rte	Baseflow alpha factor for bank storage	0	1
13	v__SLSUBBSN.hru	Average slope length	10	150
14	v__HRU_SLP.hru	Average slope steepness	0	1
15	v__CANMX.hru	Maximum canopy storage	0	100
16	v__EPCO.hru	Plant uptake compensation factor	0	1
17	v__ESCO.hru	Soil evaporation compensation factor	0	1
18	v__OV_N.hru	Manning's "n" value for overland flow	0.01	30
19	v__SURLAG.bsn	Surface runoff lag time	0	1

Note: r__ denotes the parameter value is multiplied by relative change or one plus the factor in the given range; **v__** represents the absolute change in the parameter made by substituting a parameter with a given value (Abbaspour et al., 2007).

4.2.5. Model calibration and validation

The process of comparing between the measured and simulated value is called calibration. It can be operated either manually or automatically and a combination of two. The selection is usually based on the intended purpose of the modeling. For this study, we deployed automatic SWAT CUP approaches. By using the eight most sensitive parameters that were identified in the sensitivity analysis phase and it was introduced into SWAT CUP tools from the years 2000-2009 on the monthly time step. And then, it was executed with the 500 iterations for each of eight most sensitive parameters up to fourth calibration steps. Finally, we obtained reasonable results on the third calibration steps.

Validation is normally done before the applying of the calibrated model for any further studies. It is a way of testing the model without any further adjustment of parameters as compared to an independent observed dataset. The model was validated from the years 2010-2013 on the monthly time step by taking the most optimized parameter ranges which are found in the third calibration stage.

4.2.6. Model performance evaluation

To evaluate streamflow prediction of the SWAT model, the model was simulated from 1998-2013 over Ribb watershed. The first two years (1998-1999) were taken as the warm-up period, which enables the model so as to alleviate the uncertainties existing an initial situation that are imbedded in the model (Schuol et al., 2008). These two years are not included in the analysis, but only used for model stabilization.

The model performance is evaluated at the outlet of the Ribb watershed using statistical measuring indices, those are: Nash-Sutcliffe model efficiency (NSE), coefficient of determination (R^2), percent bias (PBIAS). These can reveal the quality and the reliability of the streamflow simulation done by SWAT model as compared to the measured discharge data.

1. Nash-Sutcliffe model efficiency (NSE): it shows how well fit the plots of measured data against simulated values (Nash and Sutcliffe, 1970). Its optimum value is 1 and It can be computed as follows:

$$NSE = 1 - \left[\frac{\sum_{j=1}^{n} (Q_{Obs,j} + Q_{Sim,j})^2}{\sum_{j=1}^{n} (Q_{Obs,j} - \overline{Q_{Obs}})^2} \right] \text{.....} \quad \text{Equation 4.10}$$

2. Coefficient of determination (R^2): It also revealed the strengths of the relationship between the observed and simulated values. And then, used for quantifying the capability and reliability of the model in simulating the streamflow (Meng et al., 2014). It can be computed as follows and its optimum value is 1.

$$R^2 = \frac{\left[\sum_{j=1}^{n} (Q_{Obs,j} - \overline{Q_{Obs}}) \ (Q_{Sim,j} - \overline{Q_{Sim}}) \right]^2}{\sqrt{\sum_{j=1}^{n} (Q_{Sim,j} - \overline{Q_{Sim}})^2} \sqrt{\sum_{j=1}^{n} (Q_{Obs,j} - \overline{Q_{Obs}})^2}} \text{.....} \quad \text{Equation 4.11}$$

3. Percent bias (PBIAS): It is used for assessing the model error and indicates about water balance errors in watershed simulations (Moriasi et al., 2007). It can be computed as follows:

$$PBIAS = \frac{\sum_{j=1}^{n} (Q_{Obs,j} - Q_{Sim,j}) \ * 100}{\sum_{j=1}^{n} (Q_{Obs,j})} \quad \text{Equation 4.12}$$

Where: $Q_{Obs,j}$, $Q_{Sim,j}$ are the measured and simulated streamflow at the j^{th} time step respectively.

$\overline{Q_{Sim}}$, $\overline{Q_{Obs}}$ the average of the simulated and measured streamflow respectively; and n is the total number of observations.

4.2.7. Water availability using TRMM 3B42 and CMORPH

The common ways of evaluating the use of the satellite rainfall products for the streamflow predictions in the hydrological models can be performed by forcing the satellite rainfall datasets on the calibrated hydrological model (Bitew et al., 2012; Hughes, 2006). We also adopted this method, in order to appraise the application of satellite rainfall products for the assessment of water availability over Ribb watershed. Then, both satellite rainfall data sources were forced on the calibrated SWAT model. The modeling outputs were analyzed in the monthly time frame for considering

seasonal variations. The average monthly flow volumes were computed at the outlet of the watershed in this case lower Ribb discharge gauging station. The average monthly and annual simulated water balance components are quantified at the watershed level, which are the indicators of water availability. The major water balance components such as rainfall (PCP), surface runoff (SURF), water yield or total flow (WY), Evapotranspiration (ET), and potential Evapotranspiration (PET). Total flow or water yield is used to express the quantified amount of water that leaves from the outlet of the watershed. It can be computed as by the summation of all the contributions from surface runoff, lateral flow and groundwater to the streamflow minus of the transmission loss (Dile and Srinivasan, 2014).

CHAPTER FIVE

5. Result and Discussion

5.1. Comparison results

The area weighted of the daily rainfall at rain gauge stations and two satellite rainfall data were aggregated to the average monthly rainfall. The average monthly areal rainfall of CMORPH and TRMM 3B42 and rain gauge stations was compared at the watershed scale. The results are presented in (Figure 5.1 and Table 5.1). Based on the analysis made on average monthly from the four meteorological stations Woreta, Adiszemen, Amedber and Debretabor (2000-2013), the average monthly rainfall of the Ribb watershed is 120.98 mm. In cases of the CMORPH and TRMM 3B42 rainfall estimates from 2000-2013 analysis showed that, the average monthly rainfall of the Ribb watershed is 92.22 and 90.09 mm, respectively.

As it is illustrated in (Figure 5.1) the average monthly rainfall values for the three types of rainfall data sources. In all cases, the seasonal cycle mostly characterized by a unimodal rainfall pattern with maximum rainfall values in July over the Ribb watershed. The majority of rainfall falling in Ribb watershed during the rainy season (Jun to September) was estimated around 85.01%, on dry season about 5.84% (October to January) and on the small rainy season also occurred about 9.15% (February to May) this is based on the rainfall data from the four stations (2000-2013). The amount of rainfall on average estimated during rainy months is 308.55 mm and for dry months 21.19 mm and small rainy months 33.20 mm. Based on the TRMM 3B42 average monthly analysis result, the rainfall falling in Ribb watershed during the rainy season was accounted 78.42%, on dry season about 9.09% and on the small rainy season is about 12.50%. The rainfall amount estimated on average by this product on rainy months is 211.92 mm, dry months is 24.56 mm and small rainy

months is 33.77 mm. Based on the CMORPH average monthly analysis result also 83.87% occurred during the rainy season, on dry season about 7.20% and on the small rainy season is about 8.93%. The rainfall amount estimated on average by this product on rainy months 232.02 mm, dry months is 19.93 mm and small rainy months is 24.70 mm.

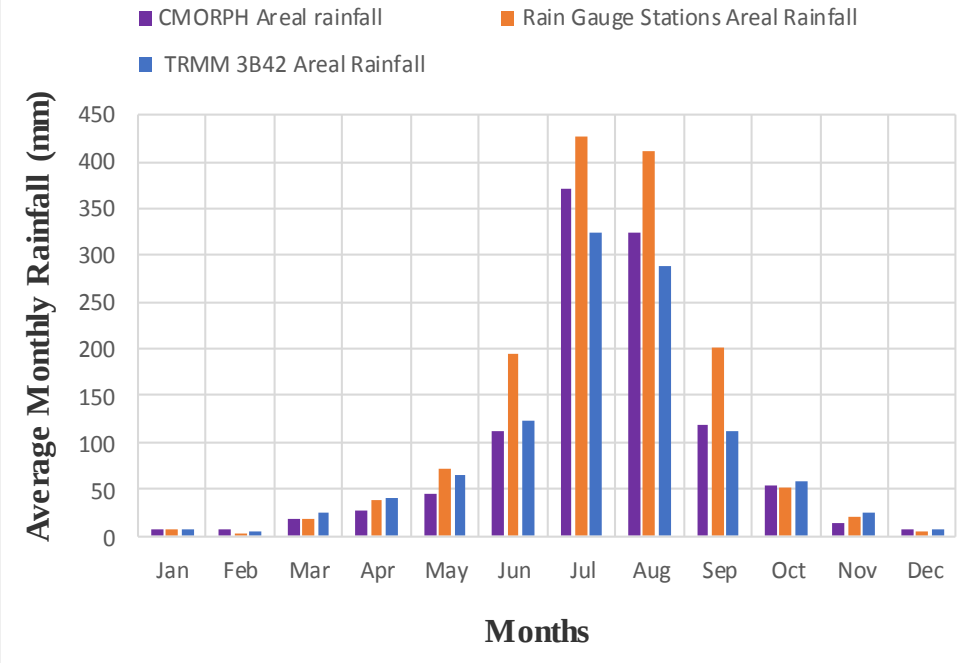

Figure 5.1 Comparison of average monthly at watershed spatial scale

The visual interpretation from (Figure 5.1) the peaks of areal rainfall of the rain gauge stations were not captured by areal rainfall of TRMM 3B42 and CMORPH this may be due to the inherent weakness of satellite rainfall products for the adequate measurement of rainfall and the second reason might be the drawback interpolation methods used that could introduces some uncertainties. TRMM 3B42 and CMORPH are portrayed slight overestimation relative to rain gauge stations during dry months, especially October, November and December.

Table 5.1 Comparison result of satellite versus rain gauge rainfall

Statistical measure indexes	TRMM 3B42 areal versus rain gauge stations areal	CMORPH areal versus rain gauge stations areal
PCC	0.99	0.99
R^2	0.98	0.97
Bias (%)	-25.54	-23.78
RMSE	57.05	45.67
RMSE %	47.00	37.75

The areal TRMM 3B42 and CMORPH rainfall had the similar highest Pearson correlation values (PCC=0.99) with the areal rainfall of the rain gauge stations. This implies that both satellite rainfall products in a good agreement with the stations rainfall at watershed and on a monthly time scale. The result of this study on the areal CMORPH rainfall versus areal rainfall of the rain gauge stations is in line with the findings of (Bitew et al., 2012) and the authors found the correlation value 0.97 for the average monthly CMORPH against gauge rainfall in the Ethiopian river basin.

In terms of the R^2 statistical measuring indexes the areal rain gauge rainfall of the stations had also the demonstrated a good agreement with the areal rainfall of two satellite products. However, the value of R^2 of the areal TRMM 3B42 greater than CMORPH rainfall. This implies that the variability of rainfall within the rain gauge stations is reasonably accounted by the TRMM 3B42 than that of CMORPH rainfall. The R^2 values obtained in this study are a bit closer to the study of (Liu et al., 2015) as they found the R^2 value with 0.98 for TRMM 3B42 whereas, for CMORPH the R^2 value of 0.94.

The bias result shows negative values that imply both satellite rainfall products were tending to underestimate of the rainfall amounts. In both cases, the level of underestimation was slightly close each other and the values can be seen in (Table 5.1). So, such kind of underestimation of the rainfall amounts and events are not desirable for flood predictions (Dembélé and Zwart, 2016).

As it is shown in (Table 5.1) the higher the value of the RMSE was observed by TRMM 3B42 than CMORPH as compared to the areal rainfall recorded by Ribb stations. From the RMSE result, it can be deduced that relatively large errors are

associated with in the TRMM 3B42 than CMORPH for this study area. These discrepancies presumptively aroused due to the errors that come from their combined retrieval algorithms and sensors used by each satellite rainfall products (Beighley et al., 2011).

On the basis of statistical indices of RMSE% result as shown in (Table 5.1), the CMORPH revealed better values than TRMM 3B42. According to (Franchito et al., 2009) when the value of RMSE% is less than 50 the satellite rainfall estimation is considered to be reliable. Hence, both satellite rainfall products are laid in the acceptable ranges of reliability values.

5.2. SWAT modeling result

5.2.1. Sensitivity and uncertainty analysis result

Eight parameters were found to be the most sensitive parameters which could have the leverage on the streamflow simulation. The level of sensitivity is evaluated based on the p-value and the absolute value of t-stat. The t-stat is always expressed in absolute value and if the parameter has larger value which mean that it is more sensitive to the streamflow. When the parameter p-value is approximated to zero, which implies it has more significance on the simulated streamflow (Abbaspour, 2012). Therefore, they are ranked in their increasing order of sensitivity shown in (Table 5.2).

Table 5.2 Results of the sensitivity analysis

S. N	Parameter Name	Values		Global sensitivity	
		Lower	Upper	t-stat	P-value
1	r__SOL_AWC(..).sol	-0.25	0.25	1.775254227	0.076489514
2	v_GW_DELAY.gw	0	500	2.099947526	0.036254796
3	v__SURLAG.bsn	0	1	2.361371627	0.018606028
4	v__GWQMN.gw	0	5000	4.698371371	3.43E-06
5	v__GW_REVAP.gw	0.02	0.2	5.489517215	6.54E-08
6	v__RCHRG_DP.gw	0	1	5.866186694	8.31E-09
7	v__CANMX.hru	0	100	6.740193838	4.55E-11
8	r__CN2.mgt	-0.25	0.25	-24.28539184	1.44E-85

Our sensitivity analysis findings corresponding with the previous studies (Alemu, 2011; Setegn et al., 2008; Tensay, 2011).

As it has been discussed in the methodology sections of sensitivity and uncertainty analysis, the model simulation, predictive uncertainty evaluated through the p-factor and r-factor indices. The satisfactory predictive uncertainty values were attained on the third calibration step as well as its subsequent validation values are shown in (Table 5.3). The optimum individual value of each predictive uncertainty index is obtained at the expenses of one over the other and also used to exhibit the strength of calibration and validation (Abbaspour et al., 2015). The authors also suggested that for streamflow simulation when the p-factor value greater 0.7 or 0.75 and for r-factor also less than 1.5 the model is satisfactory. On third calibration, we obtained the p-factor values that bracketed 85% of measured streamflow and the r-factor value equivalent to 0.65. During validation, the p-factor values was reduced, which bracketed 44% of measured streamflow and its r-factor value was pretty much improved to 0.28 since its value approached to zero is an accurate desired value. Hence, our streamflow simulation, predictive uncertainty results is in the acceptable ranges. Owing to this, the model can be used for the streamflow predictions or any other related studies can be addressed through this calibrated model.

Table 5.3 Result of predictive uncertainty indices the SWAT model

Time step	Predictive uncertainty indices	Calibration (2000-2009)	Validation (2010-2013)
Monthly	p-factor	0.85	0.44
	r-factor	0.65	0.28

5.2.2. Calibration and validation streamflow results

During the calibration process, the eight most sensitive parameters were forced into the SWAT CUP SUFI2 tool. The algorithms search for the best parameter values that maximize the objective functions in our cases (i.e. Nash–Sutcliffe efficiency) between measured and simulated streamflow on the monthly basis. Then, we obtained satisfactory results on the third calibration stage, which were judged based on the predictive uncertainty indices and statistical measuring indicators and their result (Table 6.3 and Table 6.5), respectively. The best optimized values for each of sensitive parameters are also indicated in (Table 5.4).

Table 5.4 The sensitive parameters range and their fitted values obtained on 3rd calibration

Parameter Name	Minimum Value	Maximum Value	Fitted Value
r__CN2.mgt	-0.204093	-0.018343	-0.07574
v_GW_DELAY.gw	141.613663	403.784851	154.460052
v__GWQMN.gw	2221.140625	5356.32959	3892.196289
v__GW_REVAP.gw	0.147209	0.242783	0.214015
v__RCHRG_DP.gw	-0.776831	0.076259	-0.298247
r__SOL_AWC(..).sol	-0.028407	0.211477	0.194925
v__CANMX.hru	76.87796	138.991043	122.158401
v__SURLAG.bsn	0.488635	0.981305	0.953223

Some of the calibrated parameter values, for instance the calibrated CANMX value is 122.16 which is raised beyond the allowable ranges which can be seen in (Table 5.4), while its maximum value was 100 at the end of sensitivity analysis. This could be attributed to the uniqueness of the watershed response to the spatial and hydro-climate datasets.

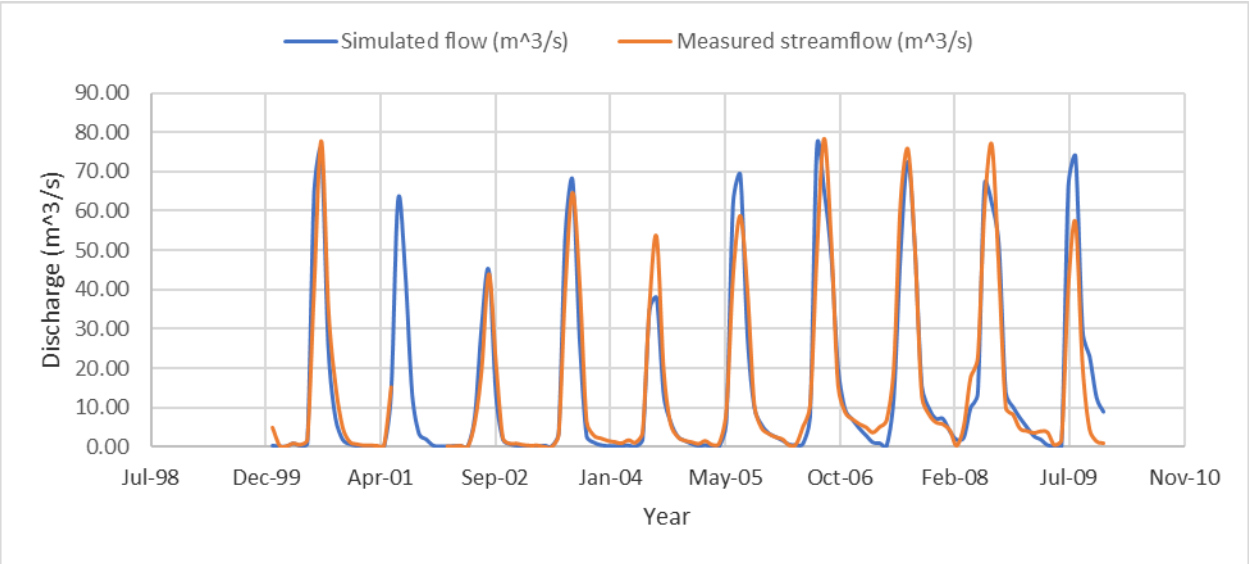

Figure 5.2 Hydrograph of measured and simulated streamflow on the 3rd calibration

In the calibration, clear disparities are depicted between the simulated and measured streamflow from June 2001 to February 2002 is because of no measured streamflow during these periods. A bit of an underestimation of the peak flows are also observed in some periods like July 2004, August 2007, August 2008 (Figure 6.2). This kind of underestimation of some of the highest events of simulated streamflow by SWAT model also seen in other studies (Garee et al., 2017; Leta et al., 2016; Sathian and Symala, 2009).

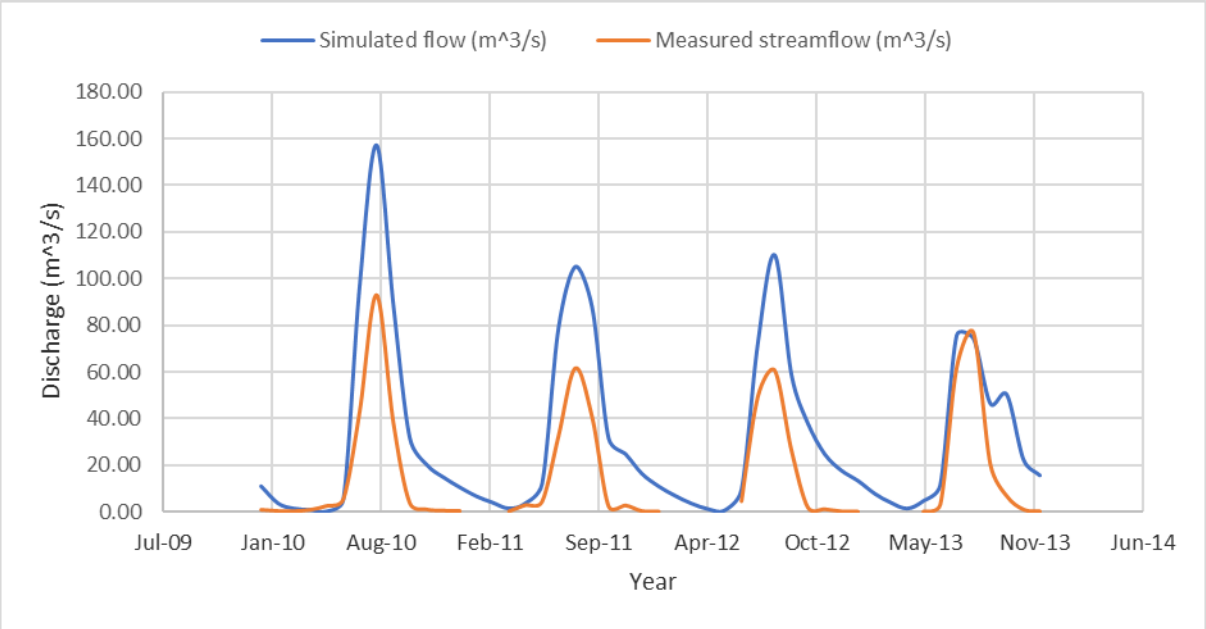

Figure 5.3 Hydrograph of measured and simulated streamflow on validation

The model performance reduction during the validation period might also happen as it has been indicated by (Lindström et al., 1997). Even if the shape of the hydrograph at the validation periods is not good as to calibration, the overall results are disclosed a very good performance of the SWAT model in capturing the hydrological responses of watershed to the given datasets at monthly time steps with acceptable predictive uncertainty ranges.

Table 5.5 Model performance statistical indicators

Time step	Statistical indicators	Calibration (2000-2009)	Validation (2010-2013)

Monthly	R^2	0.92	0.85
	NSE	0.91	0.85
	PBIAS (%)	6.1	5.8

5.2.3. Model performance

The model performance can be evaluated through statistical and graphical methods as per suggested by (Moriasi et al., 2007) model performance evaluation guidelines. The authors also stated that for streamflow simulations on the monthly time step, the model performance considered to be satisfactory: if the NSE greater than 0.50 and PBIAS less than plus or minus 25% as well as the good agreement between measured and simulated streamflow in the graphical illustration. Specifically for PBIAS values as per the model performance evaluation criteria suggested by (Van Liew et al., 2007) : if the absolute value of PBIAS less than 10% (very good), 10% less than the absolute value of PBIAS less than 15% (good); 15% less than the absolute value of PBIAS less than 25% (satisfactory), and the absolute value of PBIAS greater than or equal to 25% (unsatisfactory). Hence, our calibrated and validated model PBIAS values (see Table 5.5) are in the very good ranges.

The R^2 values approached to one indicates the perfect fit between the simulated streamflow and the measured streamflow, while R^2 greater than 0.6 is satisfactory for hydrology (Krause et al., 2005; Moriasi et al., 2007). Our calibrated and validated results of NSE and R^2 values partly in line with (Tensay, 2011) findings and the author obtained NSE and R^2 values at the monthly time step calibration and validation of the upper Ribb watershed 0.812, 0.817 and 0.800 and 0.817, respectively. On the contrary, (Dile and Srinivasan, 2014) found unsatisfactory model performances over Ribb watershed during the model simulation using conventional hydro-meteorological datasets without conducting any calibration and validation process.

The performance of the SWAT model on a monthly time step for Ribb watershed exhibited by far very good results as compared to the statistical values in the watershed model performance evaluation guidelines stated by (Moriasi et al., 2007). Even if the performance of the SWAT model is generally satisfactory, its performance as it can be seen in (Figure 6.3 and Table 6.5) is relatively reduced during the validation period. This is possibly attributed to the variations in the discharge data

used for calibration and validation periods. The simulated baseflow is smaller for calibration period, while the reverses are occurring for validation except from April-June 2010. The peaks are continuously overestimated by the model for the validation period.

5.2.4. Water availability

By using the best fitted values of the most sensitive parameter sets which are obtained from the third calibration, the streamflow simulations were performed from 2000 to 2013 using both satellite rainfall data sources. The simulated streamflow and water balance components (WBC) results are summarized in average monthly and annual basis for each satellite rainfall datasets.

6.2.4.1. Results of simulated streamflow using TRMM 3B42 and CMORPH

The simulated streamflow using TRMM 3B42 revealed sustained underestimation of for all simulation periods except during the data gaps of measured streamflow. As it can be seen in Figure 5.4 underestimation is substantial in peak flows during rainy months. Similar observation has been made by (Bitew et al., 2012) during the assessment of high resolution of satellite rainfall products for streamflow simulation at small mountainous watershed of Ethiopia. This ascribed that SWAT model is unable to capture the peak flows as it has been discussed in the model calibration discussion parts.

The rainfall assignment in SWAT model is done by relating the sub-watershed with the closest discharge gauging station nearest to its centroid. And then, when more than one rainfall data sources are existing in the sub-watershed, some of rainfall data are going to be missed. As the result of this, the SWAT model has limitations in simulating the peak streamflow (Galván et al., 2014; Pereira et al., 2016). In addition to this, the uncertainty associated with the measured discharge also one of the factors that cause these continuous underestimations of simulated streamflow's in both satellite rainfall products simulations. This was also seen (Gebregiorgis et al., 2016) and the authors stated that underestimation of large peaks in the Ribb because of the measurement problems in the Ribb discharge gauging station.

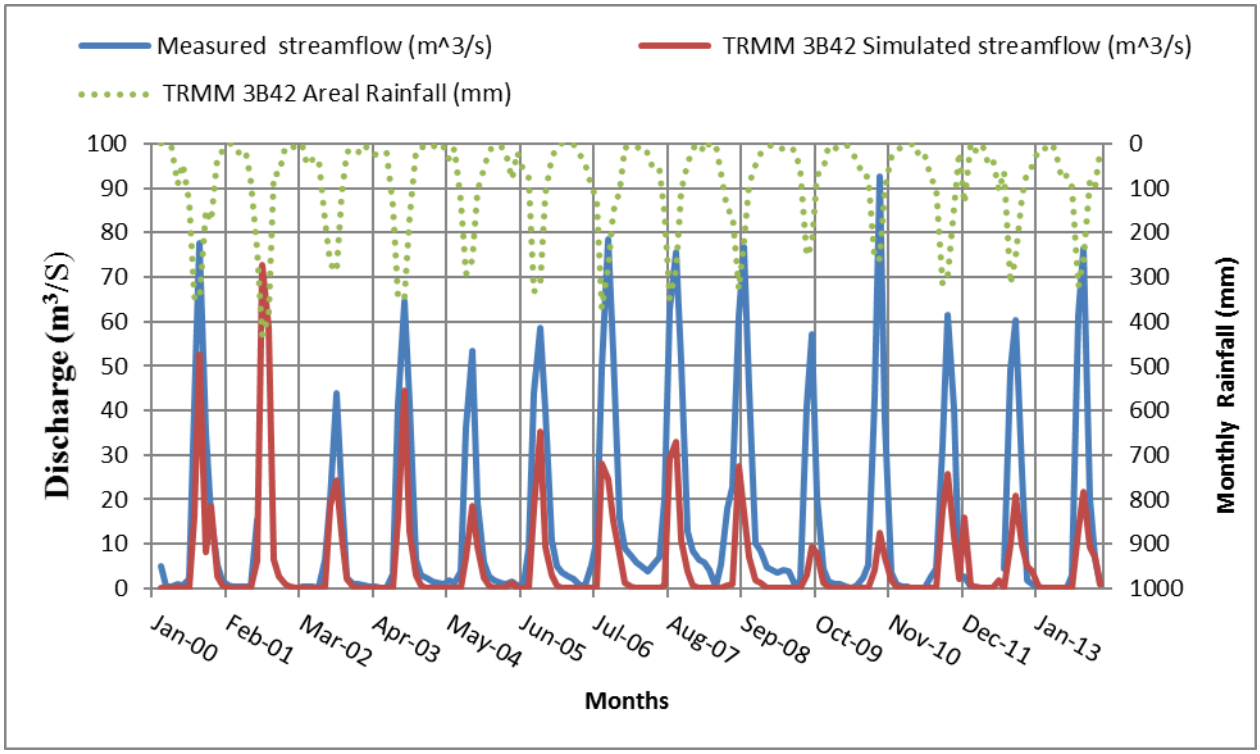

Figure 5.4 Hydrograph of measured and simulated streamflow using TRMM 3B42

Visual the comparison of the hydrograph indicated in Figure 5.5 the CMORPH based simulation also showed underestimation of the peak flows in many rainy months as well as overestimation for the month of September 2001, July 2002 and July 2012.

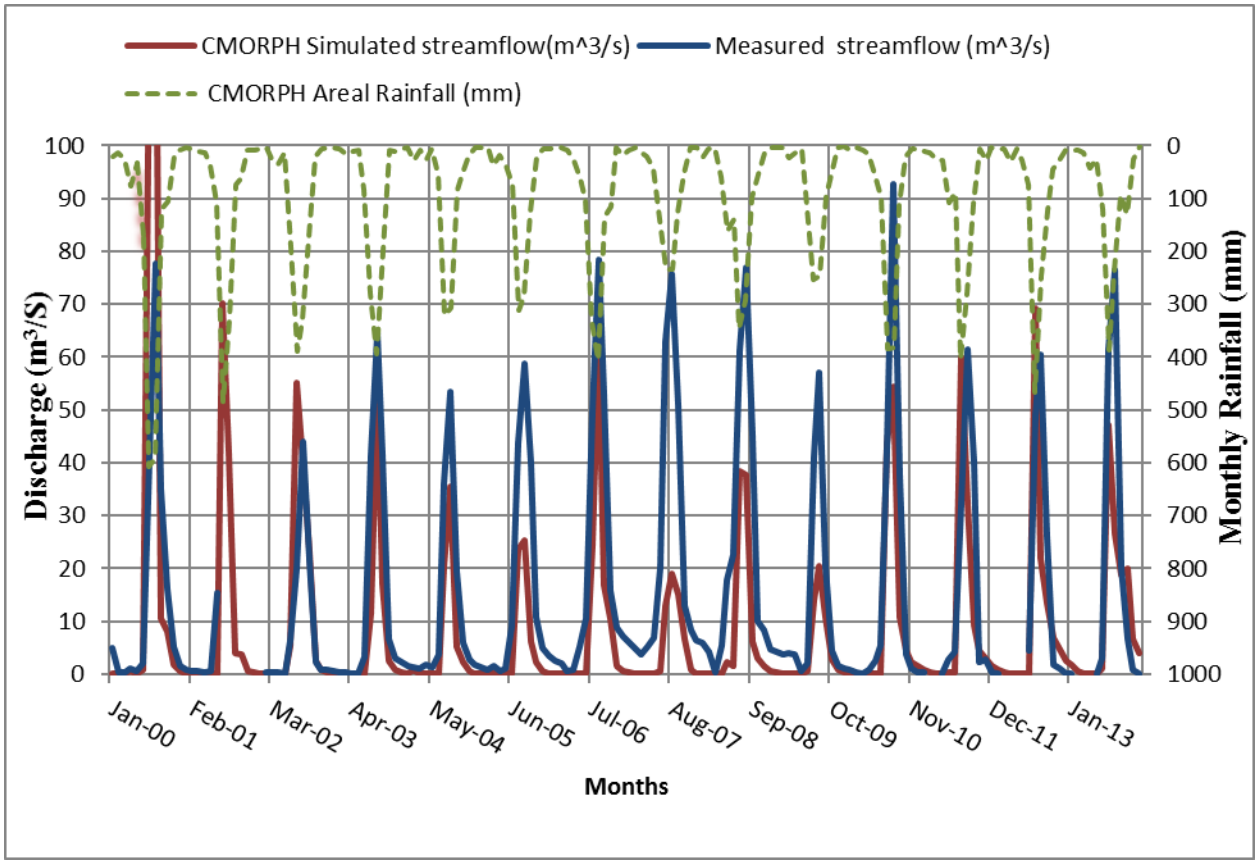

Figure 5.5 Hydrograph of measured and simulated streamflow using CMORPH

Table 5.6 Measured and Simulated streamflow using TRMM 3B42 and CMORPH

Streamflow (m^3/s)	*		* by seasons		
	Monthly	Annually	Rainy	Dry	Small rainy
Simulated by TRMM 3B42	66.34	77.4	58.92	7.03	0.39
Simulated by CMORPH	109.36	127.59	99.91	8.98	0.47
Measured	178.86	209.15	155.05	16.09	7.72

Note: * denotes the average of the streamflow data from 2000-2013

The simulated streamflow using both satellite rainfall products showed underestimations in all circumstances and the degree of underestimations can also be seen in Table 5.7. The level of underestimations especially in a small rainy season was significant in both satellite rainfall products. The incapability of the TRMM 3B42 in capturing the highest flows also seen by (Bitew and Gebremichael, 2011). However, the CMORPH showed a relatively better result as compared to the TRMM 3B42 in all cases.

Table 5.7 The degree of under prediction of streamflow using TRMM 3B42 and CMORPH

Simulated Streamflow (m^3/s)	underestimations in %		underestimations in % by seasons		
	Monthly	Annually	Rainy	Dry	Small rainy
TRMM 3B42	0.63	0.63	0.62	0.56	0.95
CMORPH	0.39	0.39	0.36	0.44	0.94

Note: It is done by average of the streamflow data from 2000-2013

6.2.4.2. SWAT simulated WBC results CMORPH and TRMM 3B42

Average monthly simulated WBC

Water balance simulation was performed using CMORPH and TRMM 3B42 rainfall products for the time periods of 14 years from 2000-2013 on the monthly time step. The results of average monthly water balance component simulations using CMORPH and TRMM 3B42 rainfall data sources are presented in Table 5.8 and Table 5.9. In both satellite rainfall product simulations, all the simulated water balance components, except potential evapotranspiration get relatively higher values during rainy months. Among the whole simulated WBC, particularly, the surface runoff, water yield and Evapotranspiration values have divulged substantial increments with respect to the raised rainfall during the months of July and August as compared to other months. On the other hand, for months, which have small rainfall amount relative to the rainy months depicted that all simulated water balance components except potential evapotranspiration gets relatively lower values. Therefore, these results are disclosed that how the rainfall greatly impacted on the overall water balance components of the watershed.

Table 5.8 Average monthly simulated WBC values using CMORPH

Month	PCP (mm)	SURF Q (mm)	LATF Q (mm)	WY (mm)	ET (mm)	PET (mm)
Jan	5.51	0	0.46	1.01	6.59	96.16
Feb	5.73	0.09	0.28	0.58	7.64	100.25
Mar	15.71	0.06	0.24	0.42	27.2	115.42
Apr	25.66	0.06	0.21	0.3	38.82	114.33
May	43.54	0.2	0.35	0.55	38.14	117.69
Jun	111.87	0.96	0.57	1.53	54.64	90.68
Jul	371.63	73.27	5.45	78.66	75.45	77.05
Aug	325.61	66.82	10.25	78.09	75	79.4
Sep	120.07	11.1	7.62	21.08	70.4	87.44
Oct	52.14	4.48	3.81	10.76	53.49	100.2
Nov	10.91	0.18	1.85	3.74	32.09	89.81
Dec	4.02	0	0.89	2.13	16.4	90.45

As it can be seen in (Table 5.8 and Table 5.9) the average monthly rainfall of the Ribb watershed using CMORPH and TRMM 3B42 satellite rainfall products is found to be 91.03 and 90.07 mm respectively. Even if the average monthly simulated WBC using both satellite rainfall product has shown up the similar trends, the simulated values of each WBC are different for each satellite rainfall products.

Table 5.9 Average monthly simulated WBC values using TRMM 3B42

month	PCP (mm)	SURF (mm)	LATF (mm)	WY (mm)	ET (mm)	PET (mm)
Jan	6.76	0.04	0.47	0.51	12.07	100.36
Feb	5.74	0.04	0.27	0.31	14.14	104.86
Mar	24.63	0.14	0.3	0.45	39.29	114.81
Apr	40.04	0.08	0.29	0.37	64.48	115.25
May	64.29	0.2	0.43	0.63	84.03	121.27
Jun	123.67	0.75	0.6	1.35	85.96	105.95
Jul	323.26	31.47	4.81	36.14	83.22	86.48
Aug	287.5	40.95	10.23	51.25	84.33	90.98
Sep	113.44	9.36	7.95	17.37	88.8	107.88
Oct	59.4	4.67	3.79	8.46	67.71	105.9
Nov	24.09	2.14	2.06	4.21	45.01	90.45
Dec	7.97	0.01	0.93	0.94	30.04	93.29

Average annual simulated WBC

SWAT model also provides the average annual computed values of WBC at the watershed scale (Table 5.10) for a given simulation period in our cases from 2000-2013 using the two satellite rainfall products. The average annual rainfall of the Ribb watershed using CMORPH and TRMM 3B42 rainfall products is found to be 1092.5 mm and 1081.00 mm respectively.

Based on the simulated average annual WBC indicated (Table 5.10) the percentage of each values can be used as indicators for water availability in Ribb watershed. Therefore, by taking the ratio of the total flow to the total rainfall for each satellite rainfall products, 11% of TRMM 3B42 rainfall simulation is converted to the total flow and 18% of CMORPH rainfall simulation is converted to the total flow. By considering the ratio of lateral flow to the total flow, the contributions of lateral flow to the total flow by the simulations of TRMM 3B42 and CMORPH is 26% and 16%, respectively. Regarding to the ratio of surface flow to the total flow, the contributions of surface flow to the total flow by the simulations of TRMM 3B42 and CMORPH is 74% and 79%, respectively. Hence, both satellite rainfall product simulations emphasize that the surface runoff contribution was by far larger than that of lateral flow contribution to the total flow of Ribb watershed. The amount of simulated Evapotranspiration with respect to the total TRMM 3B42 and CMORPH rainfall is 65% and 45% respectively. In the cases of the amount of percolation out of soil, 24% and 37% of TRMM 3B42 and CMORPH rainfall respectively were converted to percolation. For the simulated deep recharge 23% and 36% of TRMM 3B42 and CMORPH rainfall were converted to deep recharge.

Table 5.10 Average annual simulated WBC using TRMM 3B42 and CMORPH

S. N	Simulated WBC (mm)	Using	
		TRMM 3B42	CMORPH
1	LATF	32.12	31.98
2	SURF	89.85	157.25
3	WY	121.97	198.86
4	Percolation out of soil	260.59	409.13
5	ET	699.2	495.9
6	Total Recharge	252.07	395.96
7	PET	1238.5	1159.9
8	Revap from shallow aquifer	223.28	248.19

CHAPTER SIX

6. Conclusions and Recommendations

6.1. Conclusions

There had been many studies conducted in relation to the assessment of various satellite rainfall products different parts of Ethiopia large basins but not much at the watershed scale. Accordingly, in this study, primarily, we compared the amount of rainfall estimated by CMORPH and TRMM 3B42 rainfall products with the rain gauge stations on the monthly basis at Ribb watershed scale. We analyzed by using graphical and five standard statistical evaluation techniques.

From the graphical and statistical analysis, though the TRMM 3B42 and CMORPH rainfall revealed underestimation and had errors based on the result of Bias and RMSE values, respectively, they also depicted representative seasonal fluctuations and good agreement with the rain gauge station rainfall in terms of PCC and R^2 statistical results. In addition to this, based on the RMSE% statistical results, both satellite rainfall products are obtained on the acceptable ranges and can be taken as reliable satellite rainfall products. Thus, TRMM 3B42 and CMORPH rainfall products can be used for further analysis in hydro-climatology, an augment during the data gaps or when the rain gauge stations are totally not existed in Ribb and similar watersheds.

Secondly, we also evaluated the performance of the SWAT model using measured discharge data in the study area. The overall performance of the SWAT model at the monthly time step depicted very good results with acceptable predictive uncertainty ranges in calibration and validation periods. Therefore, the best fitted values of the eight most sensitive parameters which are obtained on the calibration can be used for further hydrological modeling works in the Ribb watershed and other areas which have similar hydrology, managements and climate conditions.

Finally, we appraised the water availability of the Ribb watershed in terms of simulated streamflow and the water balance components through the application of satellite rainfall products on a calibrated SWT model. Both satellite rainfall product streamflow simulations were able in capturing the measured discharge patterns of the watershed nevertheless, more of continuous underestimation was noticed. The level of underestimations is very significant at small rainy season relative to other seasons. The causes of underestimation possibly to the discharge measurement problems and the limitations of SWAT model in simulating the peak discharges. Looking at the simulated water balance components using both satellite rainfall products, the surface runoff contribution to the total flow was significant. Too much amount of water is lost by Evapotranspiration as compared to other losses throughout the simulation periods. Therefore, the simulated water balance components can also provide a valuable clue for water resources development and management.

6.2. Recommendations

The following remarks needs further investigations:

Plausible bias adjustment techniques for the specific use satellite rainfall products. For instance, in our cases, both satellite rainfall products tend to underestimate the rainfall which could not be used for forecasting the flood status in Ribb watershed unless a sort of bias improvement have been made for each product.

Types of interpolation techniques that suits for the small numbers of rain gauge stations

Other hydrological models need to be also explored for examining the application of satellite rainfall for hydrological modeling study since using the SWAT model has the limitations in the spatial representation of rainfall.

References

ABBASPOUR, K. 2012. SWAT-CUP 2012: SWAT Calibration and Uncertainty Programs-A User Manual EAWAG: Swiss Federal Institute of Aquatic Science and Technology. *Zurich, Switzerland*.

ABBASPOUR, K., JOHNSON, C. & VAN GENUCHTEN, M. T. 2004. Estimating uncertain flow and transport parameters using a sequential uncertainty fitting procedure. *Vadose Zone Journal,* 3**,** 1340-1352.

ABBASPOUR, K. C., FARAMARZI, M., GHASEMI, S. S. & YANG, H. 2009. Assessing the impact of climate change on water resources in Iran. *Water resources research,* 45.

ABBASPOUR, K. C., YANG, J., MAXIMOV, I., SIBER, R., BOGNER, K., MIELEITNER, J., ZOBRIST, J. & SRINIVASAN, R. 2007. Modelling hydrology and water quality in the pre-alpine/alpine Thur watershed using SWAT. *Journal of hydrology,* 333**,** 413-430.

ALEMU, E. 2011. EFFECTS OF WATERSHED CHARACTERISTICS ON RIVER FLOW FOR THE CASE OF RIBB AND GUMMARA, UPPER BLUE NILE. *MSc Thesis. Addis Ababa University, Ethiopia.*

ALLEN, R., PEREIRA, L., RAES, D. & SMITH, M. 1998. FAO Irrigation and Drainage Paper No. 56, Crop Evapotranspiration (Guidelines for Computing Crop Water Requirements). FAO. *Water Resources, Development and Management Service, Rome, Italy*.

BEIGHLEY, R., RAY, R., HE, Y., LEE, H., SCHALLER, L., ANDREADIS, K., DURAND, M., ALSDORF, D. & SHUM, C. 2011. Comparing satellite derived precipitation datasets using the Hillslope River Routing (HRR) model in the Congo River Basin. *Hydrological Processes,* 25**,** 3216-3229.

BIRHANE, G. 2002. Present and future water resources development in Ethiopia related to research and capacity building. *Integrated water and land management research and capacity building priorities for Ethiopia,* 11.

BITEW, M. & GEBREMICHAEL, M. 2011. Assessment of satellite rainfall products for streamflow simulation in medium watersheds of the Ethiopian highlands. *Hydrology and Earth System Sciences,* 15**,** 1147-1155.

BITEW, M. M., GEBREMICHAEL, M., GHEBREMICHAEL, L. T. & BAYISSA, Y. A. 2012. Evaluation of high-resolution satellite rainfall products through streamflow simulation in a hydrological modeling of a small mountainous watershed in Ethiopia. *Journal of Hydrometeorology,* 13**,** 338-350.

DEMBÉLÉ, M. & ZWART, S. J. 2016. Evaluation and comparison of satellite-based rainfall products in Burkina Faso, West Africa. *International Journal of Remote Sensing,* 37**,** 3995-4014.

DILE, Y. T. & SRINIVASAN, R. 2014. Evaluation of CFSR climate data for hydrologic prediction in data-scarce watersheds: an application in the Blue Nile River Basin. *JAWRA Journal of the American Water Resources Association,* 50**,** 1226-1241.

DINKU, T., CECCATO, P., GROVER-KOPEC, E., LEMMA, M., CONNOR, S. & ROPELEWSKI, C. 2007. Validation of satellite rainfall products over East

Africa's complex topography. *International Journal of Remote Sensing,* 28**,** 1503-1526.

DIRO, G., GRIMES, D., BLACK, E., O'NEILL, A. & PARDO-IGUZQUIZA, E. 2009. Evaluation of reanalysis rainfall estimates over Ethiopia. *International Journal of Climatology,* 29**,** 67-78.

DUAN, Z., BASTIAANSSEN, W. & LIU, J. Monthly and annual validation of TRMM Mulitisatellite Precipitation Analysis (TMPA) products in the Caspian Sea Region for the period 1999–2003. Geoscience and Remote Sensing Symposium (IGARSS), 2012 IEEE International, 2012. IEEE, 3696-3699.

FRANCHITO, S. H., RAO, V. B., VASQUES, A. C., SANTO, C. M. & CONFORTE, J. C. 2009. Validation of TRMM precipitation radar monthly rainfall estimates over Brazil. *Journal of Geophysical Research: Atmospheres,* 114.

GALVÁN, L., OLÍAS, M., IZQUIERDO, T., CERÓN, J. & DE VILLARÁN, R. F. 2014. Rainfall estimation in SWAT: An alternative method to simulate orographic precipitation. *Journal of hydrology,* 509**,** 257-265.

GAREDE, N. & MINALE, A. 2014. Land Use/Cover Dynamics in Ribb Watershed, North Western Ethiopia. *J. Nat. Sci. Res,* 4**,** 16.

GAREE, K., CHEN, X., BAO, A., WANG, Y. & MENG, F. 2017. Hydrological Modeling of the Upper Indus Basin: A Case Study from a High-Altitude Glacierized Catchment Hunza. *Water,* 9**,** 17.

GEBERE, S. B., ALAMIREW, T., MERKEL, B. J. & MELESSE, A. M. 2015. Performance of high resolution satellite rainfall products over data scarce parts of Eastern Ethiopia. *Remote Sensing,* 7**,** 11639-11663.

GEBREGIORGIS, A. S., MOGES, S. A. & AWULACHEW, S. B. 2016. Use of Remote Sensing-Based Precipitation Data for Flood Frequency Analysis in Data-Poor Regions. *Hydrologic Remote Sensing: Capacity Building for Sustainability and Resilience***,** 233.

GIRMA, M. M. 2013. *Potential impact of climate and land use changes on the water resources of the Upper Blue Nile Basin.* Freie Universität Berlin.

GRAYSON, R. & BLÖSCHL, G. 2001. *Spatial patterns in catchment hydrology: observations and modelling*, CUP Archive.

HAILE, A. T., RIENTJES, T., GIESKE, A. & GEBREMICHAEL, M. 2009. Rainfall Variability over mountainous and adjacent lake areas: the case of Lake Tana basin at the source of the Blue Nile River. *Journal of Applied Meteorology and Climatology,* 48**,** 1696-1717.

HONG, Y., GOCHIS, D., CHENG, J.-T., HSU, K.-L. & SOROOSHIAN, S. 2007. Evaluation of PERSIANN-CCS rainfall measurement using the NAME event rain gauge network. *Journal of Hydrometeorology,* 8**,** 469-482.

HUGHES, D. 2006. Comparison of satellite rainfall data with observations from gauging station networks. *Journal of Hydrology,* 327**,** 399-410.

JIANG, S., REN, L., HONG, Y., YONG, B., YANG, X., YUAN, F. & MA, M. 2012. Comprehensive evaluation of multi-satellite precipitation products with a dense rain gauge network and optimally merging their simulated hydrological flows using the Bayesian model averaging method. *Journal of Hydrology,* 452**,** 213-225.

KRAUSE, P., BOYLE, D. & BÄSE, F. 2005. Comparison of different efficiency criteria for hydrological model assessment. *Advances in Geosciences,* 5**,** 89-97.

LETA, O. T., EL-KADI, A. I., DULAI, H. & GHAZAL, K. A. 2016. Assessment of climate change impacts on water balance components of Heeia watershed in Hawaii. *Journal of Hydrology: Regional Studies,* 8**,** 182-197.

LIERSCH, S. 2003. The Programs dew. exe and dew02. exe: user's manual.

LINDSTRÖM, G., JOHANSSON, B., PERSSON, M., GARDELIN, M. & BERGSTRÖM, S. 1997. Development and test of the distributed HBV-96 hydrological model. *Journal of hydrology,* 201**,** 272-288.

LIU, J., DUAN, Z., JIANG, J. & ZHU, A. 2015. Evaluation of three satellite precipitation products TRMM 3B42, CMORPH, and PERSIANN over a subtropical watershed in China. *Advances in Meteorology,* 2015.

MANTAS, V., LIU, Z., CARO, C. & PEREIRA, A. 2015. Validation of TRMM multi-satellite precipitation analysis (TMPA) products in the Peruvian Andes. *Atmospheric Research,* 163**,** 132-145.

MELESSE, A., ABTEW, W. & DESALEGNE, T. Flow Analysis and Characterization of the Blue Nile River System. Proceedings of the Nile Hydrology and Ecology under Extreme Conditions Workshop, 2008. 113-126.

MELESSE, A., ABTEW, W. & SETEGN, S. G. 2014. *Nile River basin: ecohydrological challenges, climate change and hydropolitics*, Springer Science & Business Media.

MENG, J., LI, L., HAO, Z., WANG, J. & SHAO, Q. 2014. Suitability of TRMM satellite rainfall in driving a distributed hydrological model in the source region of Yellow River. *Journal of Hydrology,* 509**,** 320-332.

MOAZAMI, S., GOLIAN, S., KAVIANPOUR, M. R. & HONG, Y. 2013. Comparison of PERSIANN and V7 TRMM Multi-satellite Precipitation Analysis (TMPA) products with rain gauge data over Iran. *International journal of remote sensing,* 34**,** 8156-8171.

MORIASI, D. N., ARNOLD, J. G., VAN LIEW, M. W., BINGNER, R. L., HARMEL, R. D. & VEITH, T. L. 2007. Model evaluation guidelines for systematic quantification of accuracy in watershed simulations. *Transactions of the ASABE,* 50**,** 885-900.

NASH, J. E. & SUTCLIFFE, J. V. 1970. River flow forecasting through conceptual models part I—A discussion of principles. *Journal of hydrology,* 10**,** 282-290.

NEITSCH, S., ARNOLD, J., KINIRY, J. E. A., SRINIVASAN, R. & WILLIAMS, J. 2002. Soil and water assessment tool user's manual version 2000. *GSWRL report,* 202.

NKUNA, T. & ODIYO, J. 2011. Filling of missing rainfall data in Luvuvhu River Catchment using artificial neural networks. *Physics and Chemistry of the Earth, Parts A/B/C,* 36**,** 830-835.

OCHOA, A., PINEDA, L., CRESPO, P. & WILLEMS, P. 2014. Evaluation of TRMM 3B42 precipitation estimates and WRF retrospective precipitation simulation over the Pacific–Andean region of Ecuador and Peru.

PEREIRA, D. D. R., MARTINEZ, M. A., PRUSKI, F. F. & DA SILVA, D. D. 2016. Hydrological simulation in a basin of typical tropical climate and soil using the

SWAT model part I: Calibration and validation tests. *Journal of Hydrology: Regional Studies,* 7**,** 14-37.
PERVEZ, M. S. & HENEBRY, G. M. 2015. Assessing the impacts of climate and land use and land cover change on the freshwater availability in the Brahmaputra River basin. *Journal of Hydrology: Regional Studies,* 3**,** 285-311.
SATHIAN, K. & SYMALA, P. 2009. Application of GIS integrated SWAT model for basin level water balance. *Indian J Soil Conserv,* 37**,** 100-105.
SCHUOL, J., ABBASPOUR, K. C., YANG, H., SRINIVASAN, R. & ZEHNDER, A. J. 2008. Modeling blue and green water availability in Africa. *Water Resources Research,* 44.
SEGELE, Z. T., LAMB, P. J. & LESLIE, L. M. 2009. Large-scale atmospheric circulation and global sea surface temperature associations with Horn of Africa June–September rainfall. *International Journal of Climatology,* 29**,** 1075-1100.
SETEGN, S. G., SRINIVASAN, R. & DARGAHI, B. 2008. Hydrological modelling in the Lake Tana Basin, Ethiopia using SWAT model. *The Open Hydrology Journal,* 2.
STEDUTO, P., FAURÈS, J.-M., HOOGEVEEN, J., WINPENNY, J. & BURKE, J. 2012. Coping with water scarcity: an action framework for agriculture and food security. *Food and Agriculture Organization of the United Nations Rome*.
SUN, C. & REN, L. 2013. Assessment of surface water resources and evapotranspiration in the Haihe River basin of China using SWAT model. *Hydrological processes,* 27**,** 1200-1222.
TAFFESE, T. 2011. *Physically based rainfall: runoff modelling in the northern Ethiopian highlands: The case of Mizewa watershed.* MSc Thesis. Bahir Dar University, Ethiopia. .
TEEGAVARAPU, R. S. & CHANDRAMOULI, V. 2005. Improved weighting methods, deterministic and stochastic data-driven models for estimation of missing precipitation records. *Journal of Hydrology,* 312**,** 191-206.
TENSAY, G. 2011. Sedimentation Modeling for Ribb Dam. *MSc Thesis. Addis Ababa University, Ethiopia.*
VAN LIEW, M. W., VEITH, T. L., BOSCH, D. D. & ARNOLD, J. G. 2007. Suitability of SWAT for the conservation effects assessment project: Comparison on USDA agricultural research service watersheds. *Journal of Hydrologic Engineering,* 12**,** 173-189.
WAGNER, S., KUNSTMANN, H., BÁRDOSSY, A., CONRAD, C. & COLDITZ, R. 2009. Water balance estimation of a poorly gauged catchment in West Africa using dynamically downscaled meteorological fields and remote sensing information. *Physics and Chemistry of the Earth, Parts A/B/C,* 34**,** 225-235.
WEEDON, G., GOMES, S., VITERBO, P., SHUTTLEWORTH, W. J., BLYTH, E., ÖSTERLE, H., ADAM, J., BELLOUIN, N., BOUCHER, O. & BEST, M. 2011. Creation of the WATCH forcing data and its use to assess global and regional reference crop evaporation over land during the twentieth century. *Journal of Hydrometeorology,* 12**,** 823-848.
WMO 2011. World Meteorological Organization. *Guide to Climatological Practices,* Third edition. Geneva, Switzerland

WORQLUL, A. W., MAATHUIS, B., ADEM, A. A., DEMISSIE, S. S., LANGAN, S. & STEENHUIS, T. S. 2014. Comparison of rainfall estimations by TRMM 3B42, MPEG and CFSR with ground-observed data for the Lake Tana basin in Ethiopia. *Hydrology and Earth System Sciences,* 18**,** 4871-4881.

YANG, Y., CHENG, G., FAN, J., LI, W., SUN, J. & SHA, Y. 2013. Validation study of TMPA 3B42V6 in a typical alpine and gorge region: Jinsha River basin, China. *Natural Hazards and Earth System Sciences,* 13**,** 3479.

Appendices

Appendix A: Data used for SWAT model

Table a.1. long-term average monthly discharge (2000-2013)

Months	Discharge (m^3/s)
Jan	2.26
Feb	1.76
Mar	1.21
Apr	1.71
May	3.04
Jun	8.05
Jul	44.82
Aug	67.51
Sep	34.68
Oct	7.66
Nov	3.83
Dec	2.35

Table a.2. Long-term average monthly rainfall (1998-2013)

Station	Adiszemen	Amedber	Debretabor	Woreta
Month	PCP (mm)	PCP (mm)	PCP (mm)	PCP (mm)
Jan	7.09	3.9	11.31	3.04
Feb	0.47	1.48	3.89	2.58
Mar	5.18	8.96	26.94	3.58
Apr	21.14	35.97	44.09	18.28
May	52.63	66.05	90.24	60.41
Jun	191.68	202.22	179.09	166.14
Jul	465.94	397.39	415.86	391.02
Aug	425.31	363.38	408.27	399.53
Sep	214.61	176.11	200.61	200.31
Oct	36.14	79.23	69.89	71.19
Nov	13.73	13.35	23.43	12.73
Dec	0	2.69	7.93	2.33

Table a.3. Average monthly minimum and maximum temperature (1998-2013)

Station	Adiszemen		Woreta		Amedber		Debretabor	
months	TMin (°C)	TMax (°C)	TMin (°C)	TMax (°C)	TMin (°C)	TMax (°C)	TMin (°C)	TMax (°C)
Jan	9.18	31.05	11.08	28.66	9.27	28.10	8.04	26.60
Feb	10.43	32.62	12.25	30.41	10.89	30.10	9.34	27.80
Mar	11.55	33.06	13.04	30.69	11.67	30.71	10.29	27.80
Apr	12.12	32.68	14.03	31.40	12.23	30.86	10.73	28.50
May	13.16	32.06	14.84	30.53	12.22	29.79	10.84	28.40
Jun	12.99	28.65	14.19	27.64	10.93	27.28	10.20	28.50
Jul	12.18	25.68	13.61	24.64	10.18	23.86	9.91	28.00
Aug	12.54	25.19	13.87	24.35	10.09	23.88	9.89	24.90
Sep	12.14	27.47	13.63	25.46	9.73	25.36	9.34	26.00
Oct	10.63	29.50	12.95	27.45	9.57	26.69	8.59	27.50
Nov	9.63	29.69	11.45	28.40	9.24	27.34	7.88	27.00
Dec	8.92	30.45	10.42	28.36	8.53	27.66	7.52	26.40

Table a.4. Long-term average monthly relative humidity & solar radiation

Months	RH	Rs (MJ/ m^2/day)
Jan	45.51	19.35
Feb	42.93	21.09
Mar	38.36	22.18
Apr	51.31	21.55
May	55.82	20.90
Jun	75.14	19.76
Jul	83.46	17.27
Aug	81.77	17.86
Sep	74.71	19.23
Oct	63.71	19.50
Nov	53.72	19.23
Dec	44.15	19.00

Table a.5 Satellite Grid location

ID	GRID NAME	LAT (dd)	LON (dd)	ELEVATION (m)
1	GridA	12.125	37.625	1785
2	GridB	12.125	37.875	2194
3	GridC	12.125	38.125	2560
4	GridD	11.875	37.625	1787
5	GridE	11.875	37.875	2169
6	GridF	11.875	38.125	2594
7	GridG	11.625	38.125	2562

Table a.6. Long-term average monthly TRMM 3B42 rainfall (2000-2013)

Months	GridA (mm)	GridB (mm)	GridC (mm)	GridD (mm)	GridE (mm)	GridF (mm)	GridG (mm)
Jan	10.18	5.17	9.01	30.03	6	8.14	3.76
Feb	9.58	5.55	8.44	27.65	4.34	5.94	3.72
Mar	24.06	20.32	40.4	36.86	16.49	28.96	22.77
Apr	46.81	40.01	48.44	64.53	32.32	41.41	34.39
May	79.83	67.67	62.48	85.65	60.5	62.54	50.51
Jun	147.46	133.41	109.18	148.27	135.15	109.95	105.77
Jul	335.34	336.69	354.97	296.67	294.07	313.95	308.14
Aug	297.14	305.06	317.74	254.41	252.29	277.38	273.63
Sep	147.89	143.25	125.79	111.9	94.45	85.59	73.32
Oct	88.51	69.65	66.84	73.14	53.23	48.21	35.65
Nov	25.51	19.97	35.66	32.22	16.05	29.48	13.39
Dec	12.4	6.35	12.21	31.59	5.59	9.62	6.46

Table a.7. long-term average monthly CMORPH rainfall (2000-2013)

Months	GridA (mm)	GridB (mm)	GridC (mm)	GridD (mm)	GridE (mm)	GridF (mm)	GridG (mm)
Jan	4.5	4.06	5.1	2.18	4.18	7.85	139.07
Feb	5.47	5.08	4.44	2.58	5.66	7	114.33
Mar	25.8	21.63	16.48	14.91	10.23	11.43	136.83
Apr	27.62	28.32	29.83	24.64	21.75	23.37	153.96
May	44.48	43.67	41.85	47.2	45.96	42.38	109.08
Jun	78.47	100.7	93.53	110.09	128.04	121.47	154.1
Jul	343.79	371.84	353.91	367.81	383.34	370.75	414.55
Aug	325.49	327.37	298.51	361.84	355.7	315.05	344.87
Sep	128.95	121.85	79.97	178.85	167.92	103.52	142.93
Oct	53.16	52.3	37.64	78.96	72.25	45.17	119.07
Nov	14.81	13.46	9.63	15.54	10.18	8.63	108.49
Dec	4.53	4.02	3.87	3.09	3.12	4.42	114.36

Appendix B: SWAT simulated outputs

Table b.1. Long term average monthly measured & simulated streamflow (2000-2013) using stations rainfall

Months	Simulated streamflow (m^3/s)
Jan	4.74
Feb	2.59
Mar	1.38
Apr	0.75
May	1.47
Jun	7.57
Jul	63.79
Aug	75.69
Sep	41.39
Oct	18.21
Nov	10.53
Dec	7.26

Table b.2. Long term average monthly simulated streamflow using TRMM 3B42 V7 & CMORPH rainfall (2000-2013)

Months	TRMM streamflow (m^3/s)	CMORPH streamflow (m^3/s)
Jan	0.08	0.34
Feb	0.03	0.15
Mar	0.10	0.07
Apr	0.06	0.05
May	0.20	0.20
Jun	0.62	0.76
Jul	20.05	43.78
Aug	28.46	43.42
Sep	9.78	11.95
Oct	4.46	5.75
Nov	2.20	1.93
Dec	0.29	0.96